Mon. Not. R. Astron. Soc. **000**, 000–000 (0000) Printed 17 February 1999 (MN LATEX style file v1.4)

E and S0 galaxies in the central part of the Coma cluster: Ages, metal abundances and dark matter

Inger Jørgensen[⋆ †]

McDonald Observatory, The University of Texas at Austin, RLM 15.308, Austin, TX 78712, USA
Gemini Observatory, 670 N. A'ohoku Pl., Hilo, HI 96720, USA

Feb 17, 1999, accepted for publication in Mon. Not. Royal Astron. Soc., Gemini Preprint #42

ABSTRACT

Mean ages and metal abundances are estimated for the stellar populations in a sample of 115 E and S0 galaxies in the central $64' \times 70'$ of the Coma cluster. The estimates are based on the absorption line indices Mg_2, <Fe> and $\mathrm{H}\beta_\mathrm{G}$, and the mass-to-light ratios (M/L). Single stellar population models from Vazdekis et al. were used to transform from the measured line indices and M/L ratios to mean ages and mean metal abundances ([Mg/H] and [Fe/H]). The non-solar abundance ratios [Mg/Fe] were taken into account by assuming that for a given age and iron abundance, a [Mg/Fe] different from solar will affect the Mg_2 index but not the M/L ratio or the <Fe> and $\mathrm{H}\beta_\mathrm{G}$ indices. The derived ages and abundances are the luminosity weighted mean values for the stellar populations in the galaxies.

By comparing the mean ages derived from the Mg_2-$\mathrm{H}\beta_\mathrm{G}$ diagram to those derived from the Mg_2-M/L diagram, we estimate the variations of the fraction of dark matter. Alternatively, the difference between the two estimates of the mean age may be due to variations in the initial mass function or to any non-homology of the galaxies.

The distributions of the derived mean ages and abundances show that there are real variations in both the mean ages and in the abundances. We find an intrinsic rms scatter of [Mg/H], [Fe/H] and [Mg/Fe] of 0.2 dex, and an intrinsic rms scatter of the derived ages of 0.17 dex. The magnesium abundances [Mg/H] and the abundance ratios [Mg/Fe] are both strongly correlated with the central velocity dispersions of the galaxies, while the iron abundances [Fe/H] are uncorrelated with the velocity dispersions. Further, [Mg/H] and [Fe/H] are strongly anti-correlated with the mean ages of the galaxies. This in not the case for [Mg/Fe].

We have tested whether the slopes of the scaling relations between the global parameters for the galaxies (the Mg_2-σ relation, the <Fe>-σ relation, the $\mathrm{H}\beta_\mathrm{G}$-$\sigma$ relation and the Fundamental Plane) are consistent with the relation between the ages, the abundances and the velocity dispersions. We find that all the slopes, except the slope of the Fundamental Plane, can be explained in a consistent way as due to a combination between variations of the mean ages and the mean abundances as functions of the velocity dispersions. The slope of the Fundamental Plane is "steeper" than predicted from the variations in the ages and abundances.

Because of the correlation between the mean ages and the mean abundances, substantial variations in the ages and the abundances are possible while maintaining a low scatter of all the scaling relations. When this correlation is taken into account, the observed scatter of the scaling relations is consistent with the rms scatter in derived the ages and abundances at a given velocity dispersion.

Key words: galaxies: elliptical and lenticular, cD – galaxies: stellar content – galaxies: dark matter – galaxies: fundamental parameters

1 INTRODUCTION

The task of deriving the mean ages and the mean metal content of stellar populations from their integrated light is

⋆ E-mail: ijorgensen@gemini.edu
† Hubble Fellow.

complicated by the fact that the effects of variations in the ages and the metal content look very similar in many of the observable parameters. Older stellar populations have redder broad band visual colors than younger stellar populations, while a higher metal content also leads to redder colors. The strength of many of the metal absorption lines in the visual wavelength region react the same way; e.g., the strengths of the magnesium and iron lines increase with both age and metallicity. Thus, it is possible for two galaxies with different ages and metal content to have the same colors and strengths of the metal lines. This problem of the age-metal "degeneracy" in the observed parameters is discussed in detail by Worthey (1994). Earlier discussions of the problem were presented by, e.g., Faber (1972), O'Connell (1976), and Aaronson et al. (1978).

One of the most powerful ways of studying the stellar populations of elliptical (E) and lenticular (S0) galaxies from their integrated light is to use the strengths of the absorption lines. The Lick/IDS system (Faber et al. 1985; named after the Lick Image Dissector Scanner) of absorption line indices has been used extensively for this purpose; e.g., Burstein et al. (1984), Gorgas, Efstathiou & Aragon-Salamanca (1990), Guzmán et al. (1992), González (1993), Davies, Sadler & Peletier (1993), Fisher, Franx & Illingworth (1995, 1996), Jørgensen (1997, hereafter J97), and Kuntschner & Davies (1998).

Models have been developed that predict the line indices, the broad band colors and the mass-to-light (M/L) ratios for single stellar populations of different ages and metallicities (e.g., Worthey 1994; Weiss, Peletier & Matteucci 1995; Buzzoni 1995; Vazdekis et al. 1996; Bressan, Chiosi & Tantalo 1996; Bruzual & Charlot 1996). The models by Vazdekis et al. also give predictions for different choices of the initial mass function (IMF) of the stars. All the models except the models by Weiss et al. assume solar abundance ratios for the stars, specifically that the magnesium to iron ratio [Mg/Fe] is solar.

The models can be used to interpret the observed line indices and M/L ratios in terms of the mean ages and metallicities of the stellar populations. Worthey (1994) suggested to use the line index of one or more metal lines together with the line index of the Balmer line Hβ to break the degeneracy between age and metallicity. The Hβ line is more sensitive to the mean age of the stellar population than to its metal content. The M/L ratios of the galaxies represent another possibility for breaking the degeneracy (cf. Faber et al. 1995). In the following, we will refer to the Hβ index and the M/L ratio as the age sensitive parameters, while we will use the term metallicity sensitive parameters about the line indices for magnesium, Mg*b* and Mg_2, and the line index for iron, <Fe> (<Fe> is the average of Fe5270 and Fe5335). However, all the parameters depend on both the age and the metallicity.

Using the models, the line indices may be transformed into mean ages and metallicities by interpolation between the model values. Worthey, Trager & Faber (1995) used this technique and derived ages and metallicities for a sample of E galaxies with data from González (1993) and from the Lick/IDS data, now published by Trager et al. (1998). The sample used by Worthey et al. is not well defined and consists of a mixture of field galaxies and galaxies in groups and clusters. Worthey et al. as well as Faber et al. (1995), using mostly the same data, find large variations in the mean ages of the E galaxies.

The abundance ratios [Mg/Fe] of E and S0 galaxies show substantial variations and many galaxies have [Mg/Fe] above solar (cf. Peletier 1989; Worthey, Faber & González 1992; J97). Worthey et al. (1992) found that [Mg/Fe] could reach values of 0.3 dex above solar for the most luminous E galaxies. This is in agreement with recent results for the large sample of 250 cluster E and S0 galaxies studied by J97. The determination of the ages is complicated by the variations in [Mg/Fe]. If these variations are not taken into account, different ages (and metallicities) result from different choices of the metallicity sensitive line index. The results from Worthey et al. (1995) and Faber et al. (1995) show this effect for the indices Mg*b*, <Fe> and C4668 (C4668 is called Fe4668 by Worthey (1994), and $\mathrm{C}_2$4668 by Worthey and collaborators in publications after 1995). These authors use either C4668 or the geometrical mean of Mg*b* and <Fe>, which they name [MgFe], as the metallicity sensitive index. Kuntschner & Davies (1998) in their study of a sample of E and S0 galaxies in the Fornax cluster also used [MgFe] as the metallicity sensitive parameter and the Hβ index as the age sensitive parameter.

The use of the geometrical mean of Mg*b* and <Fe>, [MgFe], does not solve the problem posed by the variations in the abundance ratios, but rather represents a compromise given that most the models are made for solar abundance ratios. In this paper we suggest an improved method for taking into account the variations in [Mg/Fe] and deriving self-consistent estimates of ages and abundances, even when using single stellar population models derived for solar abundance ratios. Our method solves the problem that different ages and metallicities result from different choices of the metallicity sensitive line index.

The global parameters of E and S0 galaxies have been found to follow a number of tight scaling relations. The relation know as the Fundamental Plane (FP) relates the effective radius, r_e, the mean surface brightness within this radius, $<I>_\mathrm{e}$ and the (central) velocity dispersion σ, in a relation, which is linear in logarithmic space (Djorgovski & Davis 1987; Dressler et al. 1987; Jørgensen, Franx & Kjærgaard 1996, hereafter JFK96). The FP can be interpreted as a relation between the M/L ratios and the masses of the galaxies (Faber et al. 1987; Bender, Burstein & Faber 1992). This interpretation assumes that the E and S0 galaxies have similar luminosity profiles and similar dynamical structure, i.e. are homologous, such that the masses can be derived from r_e and σ. See, e.g., Hjorth & Madsen (1995) and Ciotti, Lanzoni & Renzini (1996) for discussions of the possible non-homology of E and S0 galaxies. The line indices Mg_2 and Hβ are strongly correlated with the velocity dispersions of the galaxies (e.g., Burstein et al. 1988; Fisher, Franx & Illingworth 1995; J97; Trager et al. 1998), while the <Fe> index shows a rather weak correlation with the velocity dispersion (J97; Trager et al. 1998).

The low scatter of the FP and of the relations between the velocity dispersions and the line indices can be used to set limits on the allowed variations of ages and metallicities among E and S0 galaxies. Worthey et al. (1995) found that the mean ages and metallicities derived from the line indices are correlated, in the sense that galaxies with lower mean ages have higher mean metallicities. The consequence of this relation may be that rather large age and metal variations are present while the low scatter of the scaling relations is maintained. This is discussed in a qualitative sense by Worthey et al. (1995) and Worthey (1997).

In this paper we investigate the stellar populations in E and S0 galaxies in the Coma cluster. The analysis is done on basis of a magnitude limited sample of 115 E and S0 galaxies within the central $64' \times 70'$ of the cluster. The aim is to derive the luminosity weighted mean ages and metal abundances of the galaxies, and to study how the derived parameters depend on other galaxy properties. We also establish the relation between the ages and the metallicities, and test if the variations in the ages and the metallicities are consistent with the low scatter of the scaling relations.

The sample selection and the available data are described in Sect. 2. New spectroscopic data have been obtained for part of the sample, see Appendix A. The main goals of the analysis of the data are outlined in Sect. 3. The method and the necessary assumptions are described in Sect. 4. This section also contains a discussion of how it may be possible to estimate either the variation of the fraction of dark matter (baryonic, and any non-baryonic with the same spatial distribution) in the galaxies or the variation of the slope of the IMF. Further, we determine the abundance ratios [Mg/Fe]. Sect. 5 presents the distributions of derived mean ages and abundances as well as the fraction of dark matter. In Sect. 6 we study the relations between the stellar populations and the galaxy masses, luminosities and velocity dispersions. The relation between the derived ages and the abundances is presented in Sect. 7. In Sect. 8 we discuss the implications for the scaling relations. The conclusions are summarized in Sect. 9.

2 SAMPLE SELECTION AND DATA

Jørgensen & Franx (1994) presented CCD photometry in Gunn r for a magnitude limited sample of 173 galaxies within the central $64' \times 70'$ of the Coma cluster. The sample was selected based on magnitudes from Godwin, Metcalfe & Peach (1983, hereafter GMP). There are 146 E and S0 galaxies in the sample, as classified by Dressler (1980). The sample has a magnitude limit of $\hat{r} = 15\overset{\mathrm{m}}{.}1$, where $\hat{r} = b - (b - r)$ is derived from the b magnitudes and the colors given in GMP. Jørgensen & Franx (1994) derived the effective radius, r_e, the mean surface brightness within this radius, $<\mu>_\mathrm{e}$. Jørgensen, Franx & Kjærgaard (1995a, hereafter JFK95a) give seeing corrected values for these parameters, which we will use in the present study. The total magnitude can be calculated from r_e and $<\mu>_\mathrm{e}$ as $m_\mathrm{T} = <\mu>_\mathrm{e} - 5 \log r_\mathrm{e} - 2.5 \log 2\pi$.

Spectroscopic observations of 44 galaxies in the sample were obtained with the McDonald Observatory 2.7-m Telescope equipped with the Large Cassegrain Spectrograph (LCS). The reductions of these data are described in Appendix A, which also contains the determination of the central velocity dispersions, and the line indices Mg_2, <Fe>, and $\mathrm{H}\beta_\mathrm{G}$. We use the passbands for the line indices as given by Worthey et al. (1994), except for $\mathrm{H}\beta_\mathrm{G}$ which is defined by J97 (see also González 1993).

Observations of 38 galaxies in the sample were obtained with the McDonald Observatory 2.7-m Telescope equipped with the Fiber Multi-Object Spectrograph (FMOS). FMOS is a grism spectrograph with 90-100 fibers and a field of view of 66 arcmin diameter. The spectra were obtained as part of a program to measure redshifts of fainter galaxies in the Coma cluster. The reductions and determination of the redshifts are described in detail in Jørgensen & Hill (1998). Here we use the high signal-to-noise spectra obtained of the bright galaxies in the present sample of E and S0 galaxies. Appendix A describes how the line indices derived from these spectra were calibrated to the Lick/IDS system.

Further, we use the velocity dispersions and Mg_2 indices as given by Jørgensen, Franx & Kjærgaard (1995b, hereafter JFK95b) for a total of 72 galaxies. These data are from from Davies et al. (1987) [33 galaxies], Dressler (1987) [36 galaxies], Lucey et al. (1991) [25 galaxies] and Guzmán et al. (1992) [23 galaxies]. JFK95b calibrated the data to a consistent system and derived mean values based on all available measurements.

In order to increase the number of galaxies for which $\mathrm{H}\beta_\mathrm{G}$ is available, we have transformed the $\mathrm{H}\delta$ strengths determined by Caldwell et al. (1993) to $\mathrm{H}\beta_\mathrm{G}$. The details of this transformation are described in Appendix A. We use $\mathrm{H}\beta_\mathrm{G}$ derived from $\mathrm{H}\delta$ only for those 22 galaxies with no direct measurement of $\mathrm{H}\beta_\mathrm{G}$.

Velocity dispersions are available for 116 E and S0 galaxies. The absorption line index Mg_2 is available for 115 of those galaxies; a sub-sample of 93 galaxies have measured $\mathrm{H}\beta_\mathrm{G}$ indices, and <Fe> have been measured for 71 of those galaxies. The Mg_2 and <Fe> line indices are on the Lick/IDS system. The $\mathrm{H}\beta_\mathrm{G}$ index is related to the Lick/IDS $\mathrm{H}\beta$ index as $\mathrm{H}\beta_\mathrm{G} = 0.866\mathrm{H}\beta + 0.485$ (J97). The $\mathrm{H}\beta_\mathrm{G}$ index can be strongly affected by emission. This would lead to a weaker $\mathrm{H}\beta_\mathrm{G}$ index and therefore an overestimation of the age. The $\mathrm{H}\beta_\mathrm{G}$ indices used in this paper are not corrected for emission. We used the spectra themselves and as well as the residual spectra after subtraction of the template stellar spectra used for the determination of the velocity dispersion to test for the presence of emission lines. Only three of the galaxies in the sample have significant emission lines, GMP 4156, GMP 4315 and GMP 4918. With the available S/N of the spectra, we can detect emission in galaxies if the equivalent width of [OIII]5007Å is larger than about 0.5Å.

All the spectroscopic parameters are centrally measured values corrected to a circular aperture with a diameter of $1.19\,\mathrm{h}^{-1}\,\mathrm{kpc}$ (JFK95b; J97), $H_0 = 100\,\mathrm{h\,km\,s^{-1}\,Mpc^{-1}}$. The line indices are corrected for the effect of the velocity dispersion (see JFK95b; J97). We adopt the technique for aperture correction described by JFK95b and J97. These aperture corrections are derived for mean values of the radial gradients of the velocity dispersions and the line indices. Carollo, Danziger & Buson (1993) and González & Gorgas (1995) found that the radial gradients of Mg_2 correlate with the central values of Mg_2 and with the galaxy mass. The correlations are strongest for galaxies with masses below $10^{11}\,\mathrm{M}_\odot$ (for $H_0 = 75\,\mathrm{km\,s^{-1}\,Mpc^{-1}}$) and Mg_2 smaller than about 0.25. For galaxies with with Mg_2 in the interval 0.2–0.34 the average radial gradient, $\Delta\,\mathrm{Mg}_2/\Delta\log r$, varies between -0.03 and -0.07 (González & Gorgas 1995). Only three galaxies in our sample have Mg_2 smaller than 0.2, and two of those have emission lines and are therefore excluded from our analysis. Our adopted aperture correction for Mg_2, $\Delta\mathrm{Mg}_2 = \xi \log d_\mathrm{ap}/d_\mathrm{norm}$, has $\xi = 0.04$ for an average radial

Table 1. Model predictions from Vazdekis et al. (1996)

Model relation			rms
Mg_2	$\approx$	$0.12 \log \mathrm{age} + 0.18[\mathrm{M/H}] + 0.14$	0.008
$\log$ <Fe>	$\approx$	$0.13 \log \mathrm{age} + 0.26[\mathrm{M/H}] + 0.34$	0.008
$\log \mathrm{H}\beta_{\mathrm{G}}$	$\approx$	$-0.27 \log \mathrm{age} - 0.13[\mathrm{M/H}] + 0.52$	0.007
$\log M/L_r$	$\approx$	$0.67 \log \mathrm{age} + 0.24[\mathrm{M/H}] - 0.20$	0.020

Note – $[\mathrm{M/H}] \equiv \log Z/Z_{\odot}$ is the total metallicity relative to solar. The relations were derived as least squares fits to the model values for ages of 2 Gyr or larger.

gradient of -0.059 (JFK95b). With radial gradients between -0.03 and -0.07 we would therefore expect ξ to vary between 0.02 and 0.05. The aperture diameters, d_{ap}, for all the data used in this paper, are between $2\farcs6$ (our FMOS data) and $4\farcs56$ (the LCOHI data from Davies et al. 1987), while $d_{\mathrm{norm}} = 3\farcs4$ (cf. JFK95b). Using $\xi = 0.04$ for all the galaxies would result in the aperture corrections being incorrect with no more than ± 0.0026. The expected rms scatter in the corrected Mg_2 values introduced by using the average aperture correction is even smaller. Since the radial gradients of $\log$ <Fe> and $\log \mathrm{H}\beta_{\mathrm{G}}$ are similar or smaller than those of Mg_2, we expect any effects on these indices due to the adopted aperture correction to be similarly small. Thus, it is safe to ignore these effects in the following analysis.

Comparisons of the spectroscopic data from the different sources as well as the adopted average spectroscopic parameters are presented in Appendix A.

The sample of 115 E and S0 galaxies with both spectroscopy (velocity dispersion and Mg_2) and photometry available is 93% complete to a total magnitude of $15\fm05$ in Gunn r. There are 9 fainter galaxies in the sample. All the spectroscopic parameters (σ, Mg_2, <Fe>, and $\mathrm{H}\beta_{\mathrm{G}}$) are available for 71 of the galaxies, three of which have emission lines. This subsample is 61% complete to a total magnitude of $15\fm05$ in Gunn r.

3 OUTLINE OF THE GOAL

The main idea is to use the M/L ratios, and the $\mathrm{H}\beta_{\mathrm{G}}$, Mg_2 and <Fe> indices to derive the luminosity weighted mean ages and the mean abundances [Mg/H] and [Fe/H]. Ideally, we also want to derive the slope of the IMF, the fraction of dark matter in the galaxies, and an estimate of the non-homology. Single stellar population models (e.g., Worthey 1994; Vazdekis et al. 1996) relate the line indices and the M/L ratios (of the stellar population) to the ages, the metallicities and the slope of the IMF. The transformation from the observables (M/L, $\mathrm{H}\beta_{\mathrm{G}}$, Mg_2, and <Fe>) to the physical parameters (ages, [Mg/H] and [Fe/H]) is done by interpolation between the model predictions (see also, Milvang-Jensen & Jørgensen, 1998, in prep.). By using single stellar population models we are effectively measuring the luminosity weighted mean values of the physical parameters. Thus, we do not get any detailed information about the star formation history of the galaxies.

In the following, we use the models from Vazdekis et al. (1996). Table 1 summarize the approximate relations between the physical parameters and the observables for some of these models. The IMF for the models is the so-called "bi-modal" IMF. This IMF resembles a Scalo (1986) IMF, with a shallow low-mass slope and a steep high-mass slope. For the models in Table 1 we use the IMF with a high-mass slope of $x = 1.35$, which is the same as the the slope of the Salpeter (1955) IMF. The $\mathrm{H}\beta_{\mathrm{G}}$ index and the M/L ratio are both more sensitive to the age of the stellar population than the metallicity. The opposite is the case for the Mg_2 and <Fe> indices. Section 4 discusses how we take the variations of [Mg/Fe] into account, even though the models were made for solar [Mg/Fe].

We derive the M/L ratios from the effective radii, the central velocity dispersions and the luminosities. We assume that the total mass (baryonic, and any non-baryonic matter with the same spatial distribution) can be derived as $\mathrm{Mass} = 5\sigma^2 r_{\mathrm{e}} \mathrm{G}^{-1}$. We adopt this formula from Bender et al. (1992) who derived it based on King (1966) models and under the assumption of an isotopic velocity dispersion. The exact value of the proportionality constant in the equation is not critical for our results.

The M/L ratio in solar units is then given as $\log M/L = 2\log\sigma - \log \langle I \rangle_{\mathrm{e}} - \log r_{\mathrm{e}} - 0.73$, where r_{e} is in kiloparsec (we use a Hubble constant of $H_0 = 50\ \mathrm{km\,s^{-1}\,Mpc^{-1}}$) and σ is in $\mathrm{km\,s^{-1}}$. We refer to these M/L ratios as "measured" M/L ratios. The M/L ratios can be measured to within a factor only. This is partly due to the uncertainty of H_0 and partly due to the uncertainty of relating the mass to the measured effective radius and central velocity dispersion. Variations in the slope of the IMF are reflected mainly in the M/L ratios and cause only small changes in the line indices, see also J97. Variations in the fraction of dark matter affect only the M/L ratios. Further, any non-homology of the galaxies will affect the measured M/L ratios, but not the line indices. We cannot with the present data disentangle these three effects. We can either estimate the fraction of dark matter (baryonic, and any non-baryonic matter with the same spatial distribution) under the assumption that the IMF is the same for all the galaxies, or we can estimate the slope of the IMF under the assumption that the fraction of dark matter does not vary from galaxy to galaxy. We have no simple way of parameterizing the possible non-homology of the galaxies.

Once the ages, the abundances and the dark matter fractions (or the slopes of the IMF) have been derived, we investigate the distributions of these parameters and their dependency on the velocity dispersion, the masses and the luminosities of the galaxies. We establish the relations between the mean ages, the mean abundances and the velocity dispersions of the galaxies. Finally we test if the slopes and the scatter of the scaling relations are consistent with the relations between the ages and the abundances and with the scatter of the derived mean ages and abundances.

Throughout this paper, we will treat E and S0 galaxies as one class of galaxies. This is supported by the results from Jørgensen & Franx (1994). Using the same photometric data as used in this paper, Jørgensen & Franx found that E and S0 galaxies fainter than $M_{r_{\mathrm{T}}} = -23\fm1$ (absolute magnitude in Gunn r for $H_0 = 50\ \mathrm{km\,s^{-1}\,Mpc^{-1}}$) form one class of galaxies with a broad distribution of the relative disk luminosities, $L_{\mathrm{D}}/L_{\mathrm{tot}}$, between zero (no disk) and one (all disk). The change in $L_{\mathrm{D}}/L_{\mathrm{tot}}$ was found to be continuous, i.e., the E and S0 galaxies do not have a bi-modal distribution in $L_{\mathrm{D}}/L_{\mathrm{tot}}$. J94 also found that the classification of a galaxy depends strongly on its inclination; face-on galaxies are more likely to be classified as E galaxies, while edge-on

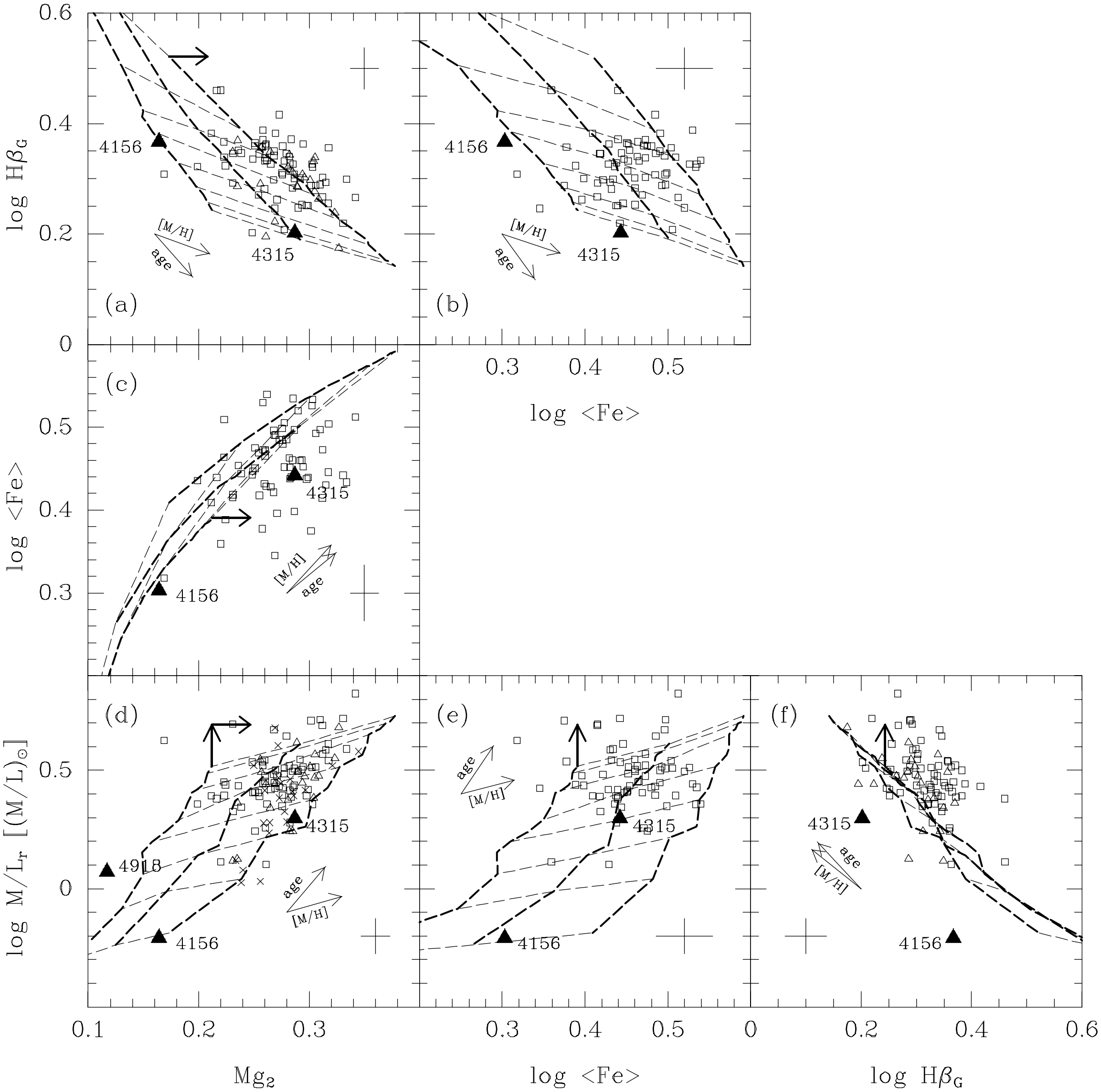

Figure 1. The line indices and the M/L ratio versus each other. Boxes – galaxies with all parameters available; triangles – galaxies with available $H\beta_G$ but without measured <Fe>; crosses – galaxies with without measured <Fe> and $H\beta_G$; filled triangles – emission line galaxies. Single stellar population models from Vazdekis et al. (1996) are overplotted. The models have a bi-modal IMF with a high-mass slope of $x = 1.35$. Thick dashed lines – constant metallicity ([M/H] $= -0.4, 0.0, 0.4$); thin dashed lines – constant ages (1, 2, 3, 5, 8, 12, 15 and 17 Gyr). The thin arrows on each panel indicate the direction of increasing age and [M/H], respectively. Typical error bars are given on the panels. The arrows on panels (a) and (c)-(f) show the apparent shifts of the models relative to the data when the adopted offsets in Mg_2 and $\log M/L$ are applied. We offset the data with $\Delta Mg_2 = -0.035$ and $\Delta \log M/L = -0.175$.

galaxies are classified as S0 galaxies. As a consequence, the traditional classes of E and S0 galaxies are not well defined. None of the galaxies brighter than $M_{r_T} = -23\overset{m}{.}1$ showed any signs of disks (Jørgensen & Franx 1994). In this paper we will comment on how the properties of these bright galaxies compare with the properties of the fainter galaxies, and we will make a few comparative comments regarding E and S0 galaxies. A larger discussion of E versus S0 galaxies and the possible relations between L_D/L_{tot} and the ages and abundances is beyond the scope of this paper and will be included in a future paper (Milvang-Jensen & Jørgensen, 1998, in prep.).

4 THE METHOD AND THE ASSUMPTIONS

Fig. 1 shows the line indices versus each other and versus the M/L ratio. Overplotted on the panels are the stellar population models from Vazdekis et al. (1996) with a bi-modal IMF with a high-mass slope of $x = 1.35$. The models are made for solar abundance ratios, specifically for [Mg/Fe]=0. Further, the M/L ratios are those of the stellar populations. Any dark matter in the galaxies has not been taken into account. In order to use these models, we need to make assumptions about how to handle the non-solar [Mg/Fe], the possible offset in the M/L ratios, and any variations in the fraction of dark matter.

Tripicco & Bell (1995) have studied how the line indices react to changes in the abundances of various elements, and to changes in the overall metallicity [M/H]. They find that for cool giant stars Mg_2 depends mostly on [Mg/H] (and [C/H]) and to a lesser extent on [Fe/H]. Mg_2 depends stronger on [Mg/H] than on the overall metallicity [M/H]. The <Fe> index, which is the average of the indices Fe5270 and Fe5335, is equally sensitive to changes in [Fe/H] and to changes in [M/H]. The Hβ index is found to weaken slightly with higher metallicity. Weiss et al. (1995) derive stellar population models for non-solar abundance ratios, [Mg/Fe]$\neq$0. They show that the luminosities (and therefore the M/L ratios) are not significantly different for models with solar abundance ratios and those with [Mg/Fe]>0, for a given overall metallicity. Based on these results, we make the following assumptions.

(a) The iron abundance [Fe/H] and the ages can be measured from the Hβ_G-<Fe> diagram (Fig. 1b).

(b) The measured M/L ratios are on average correct to within a factor. We therefore apply an offset to $\log M/L$ to achieve the best agreement on average between ages and [Fe/H] derived from the Hβ_G-<Fe> diagram (Fig. 1b) and from the M/L-<Fe> diagram (Fig. 1e).

(c) For a given age and [Fe/H], an abundance ratio [Mg/Fe] different from zero will affect the Mg_2 index but not the <Fe> and Hβ_G indices or the M/L ratio (cf. Tripicco & Bell 1995; Weiss et al. 1995). To derive the magnesium abundance we first apply an offset to the Mg_2 indices that gives the best agreement between the ages and metallicities [M/H] derived from the M/L-<Fe> diagram (Fig. 1e) and the M/L-Mg_2 diagram (Fig. 1d), and between the ages and metallicities derived from the Hβ_G-<Fe> diagram (Fig. 1b) and the Hβ_G-Mg_2 diagram (Fig. 1a). We then derive the metallicities [M/H] and the ages. Because the Mg_2 index for a given age depends on the metallicity [M/H] as $\mathrm{Mg}_2 \approx 0.18\,[\mathrm{M/H}]$ (cf. Table 1), we finally derive the magnesium abundance as [Mg/H]=[M/H]–$\Delta\mathrm{Mg}_2/0.18$.

(d) The differences between ages derived using the Hβ_G indices and the M/L ratios, respectively, reflect variations in either the fraction of dark matter in the galaxies or in the IMF slope, see also Section 4.1.

The adopted offsets are $\Delta \log M/L = -0.175$ and $\Delta\mathrm{Mg}_2 = -0.035$, which were added to the data before the ages and metallicities were derived. The arrows on Fig. 1 show the offsets as the apparent move of the models relative to the data, when the offsets are applied.

After adding the offsets, we derive the ages and metallicities by interpolation in the Hβ_G-<Fe> diagram, Hβ_G-Mg_2 diagram, M/L-<Fe> diagram, and M/L-Mg_2 diagram. This gives four estimates of the luminosity weighted ages, two estimates of the iron abundance [Fe/H], and two estimates of the magnesium abundance [Mg/H]. The uncertainties were derived by adding and subtracting the uncertainties of the measured parameters and rederiving the ages and metallicities. In each case half the maximum difference between the values derived from these determinations was used as the uncertainty.

Fig. 2 shows the four age estimates versus each other. The estimates of [Fe/H] and [Mg/H] are shown versus each other in Fig. 3. These two figures will be discussed in detail in Sections 4.1 and 4.2, respectively.

One may argue that it would have been more straight forward to derive [Mg/H] directly from the Hβ_G-Mg_2 diagram and the M/L-Mg_2 diagram. However, such determinations would have resulted in a systematic disagreement between the ages derived from the Hβ_G-<Fe> diagram and the Hβ_G-Mg_2 diagram, and between the ages derived from the M/L-<Fe> diagram and M/L-Mg_2 diagram. The ages derived using Mg_2 would be systematicly smaller than those derived using <Fe>. This problem was discussed by Worthey et al. (1995) and Worthey (1996). By using the method described in the assumptions (a)–(c) we avoid the inconsistency in the derived ages and can determine all the parameters ([Mg/H], [Fe/H], [Mg/Fe] and ages) in a self-consistent way.

4.1 The dark matter, the IMF, and the non-homology

The age estimates based on the Mg_2-M/L diagram agree within the uncertainties with those based on the <Fe>-M/L diagram, see Fig. 2. Similarly, the ages derived from the Mg_2-Hβ_G diagram agree with those derived from the <Fe>-Hβ_G diagram. However, the ages based on the Mg_2-M/L diagram deviate from those based on the Mg_2-Hβ_G diagram, and the ages from the <Fe>-M/L diagram deviate from those derived from the <Fe>-Hβ_G diagram. Because we detect emission in only three of the galaxies in the sample, it is highly unlikely that the difference in the age estimates is caused by Hβ_G being strongly contaminated by emission, cf. Section 2.

The differences $\log \mathrm{age}_{\mathrm{Mg}_2,M/L} - \log \mathrm{age}_{\mathrm{Mg}_2,\mathrm{H}\beta_\mathrm{G}}$ and $\log \mathrm{age}_{<\mathrm{Fe}>,M/L} - \log \mathrm{age}_{<\mathrm{Fe}>,\mathrm{H}\beta_\mathrm{G}}$ are tightly correlated. (The subscripts on the ages refer to the diagrams from which they were derived). The differences are also correlated with the residuals relative to the Hβ_G-M/L relation established by J97. This indicates that the ages based on the Hβ_G indices differ from those based on the M/L ratios because of variations in the measured M/L ratios at a given Hβ_G. Variations in Hβ_G due to variations in the ages and/or metallicities cannot be the cause of the difference, since such variations would also cause variations in the M/L ratios and would move the data points along the Hβ_G-M/L relation rather than away from it (cf. Fig. 1, see also J97).

We first interpret the differences in the age estimates as due to variations in the fraction of dark matter. Thus, we assume that the IMF is the same for all the galaxies and that the total masses can be derived as $M = c_1 \sigma^2 r_\mathrm{e}$, where c_1 is a constant. We then use the approximate relation between the M/L ratio, the age and the metallicity (Table 1) to translate the age differences into variations in the fraction of dark matter. Because the total masses include both baryonic and any non-baryonic matter with the same spatial distribution, the dark matter fractions discussed in the following will include both baryonic dark matter and any

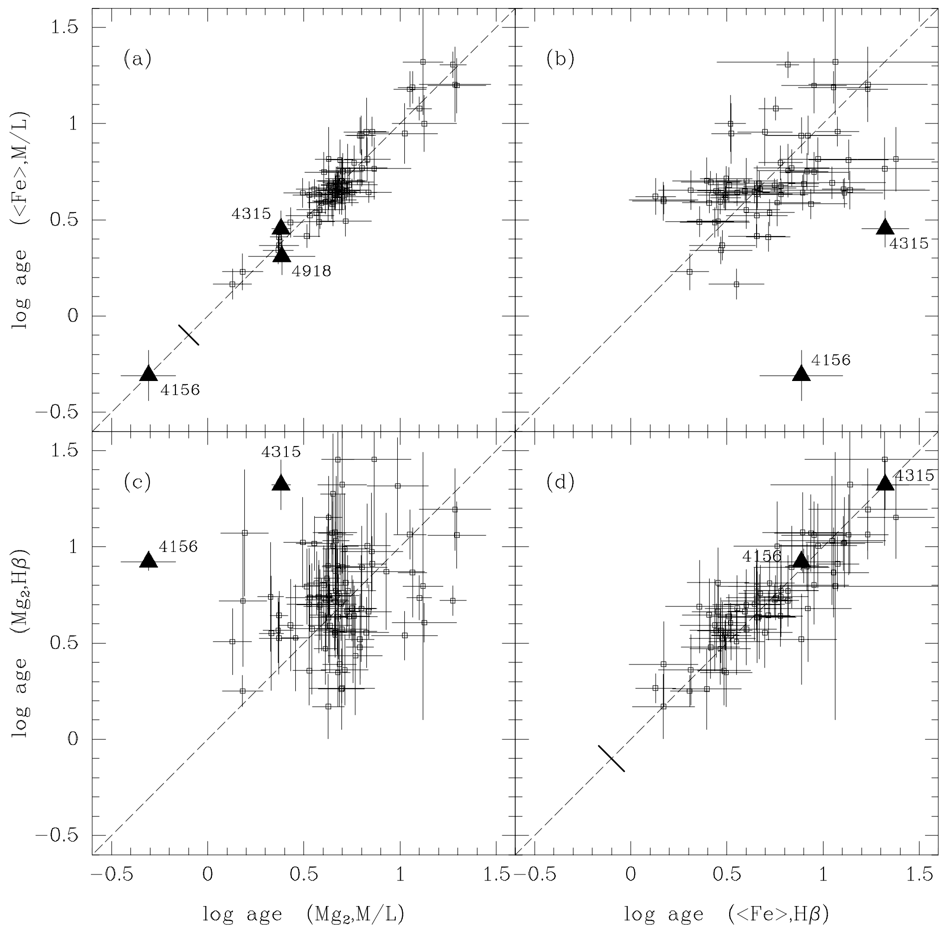

Figure 2. The four estimates of log age versus each other. The parameters in parentheses refer to the diagram from which the ages were derived. Filled triangles – emission line galaxies. Dashed lines – one-to-one relations. The thick solid lines on panels (a) and (d) at $(-0.1, -0.1)$ show the median measurement error relative to the one-to-one relation when the correlations of the measurement errors have been taken into account.

non-baryonic dark matter with the same spatial distribution. Figs. 3(b)-(c) show that the derived metallicities do not depend significantly on whether the M/L ratio or the $H\beta_G$ index was used. Thus, the difference in derived ages can be expressed as a offset in the M/L ratio as

$$\Delta \log M/L = 0.67 \left(\log \mathrm{age}_{\mathrm{Mg}_2,M/L} - \log \mathrm{age}_{\mathrm{Mg}_2,\mathrm{H}\beta_\mathrm{G}} \right) \quad (1)$$

here written for the age estimates where Mg_2 index was used as the metallicity sensitive parameter. Further, the measured M/L ratio, after being offset with -0.175 (cf. Section 4), can be written as

$$\log M/L_{\mathrm{meas}} = \log M/L_{\mathrm{lum}} + \Delta \log M/L \quad (2)$$

where M/L_{lum} is the M/L ratio of the stars that would give a one-to-one relation between the ages based on the M/L ratios and those based on the $H\beta_G$ indices. Since the measured M/L ratio is only accurate to within a factor, cf. Section 3, the true M/L ratio is

$$\log M/L_{\mathrm{true}} = \log \left(f \cdot M/L_{\mathrm{meas}} \right) \quad (3)$$

The true mass is the sum of the luminous mass, M_{lum} and dark matter, M_{dark}. From equations (1)-(3) we get

$$\log \left(\frac{M_{\mathrm{dark}}}{M_{\mathrm{lum}}} + 1 \right) = \Delta \log M/L + \log f \quad (4)$$

Second, we assume that the fraction of dark matter does not vary from galaxy to galaxy. We can then interpret the differences in the two age estimates as due to differences in the slope of the IMF. Using the models from Vazdekis et al. (1996) that have bi-modal IMFs we find the following relation for photometry in Gunn r

$$\log M/L_r \approx (0.91 - 0.18x) \log \mathrm{age} + 0.24[\mathrm{M/H}] - 0.78 + 0.43x \quad (5)$$

where x is the high-mass slope of the IMF. For $x = 1.35$, equation (5) is equivalent to the last equation in Table 1. The age estimates $\mathrm{age}_{\mathrm{Mg}_2,M/L}$ were based on an IMF with $x = 1.35$. The key assumption in order to derive the slope of the IMF is that if the model with the correct slope had been

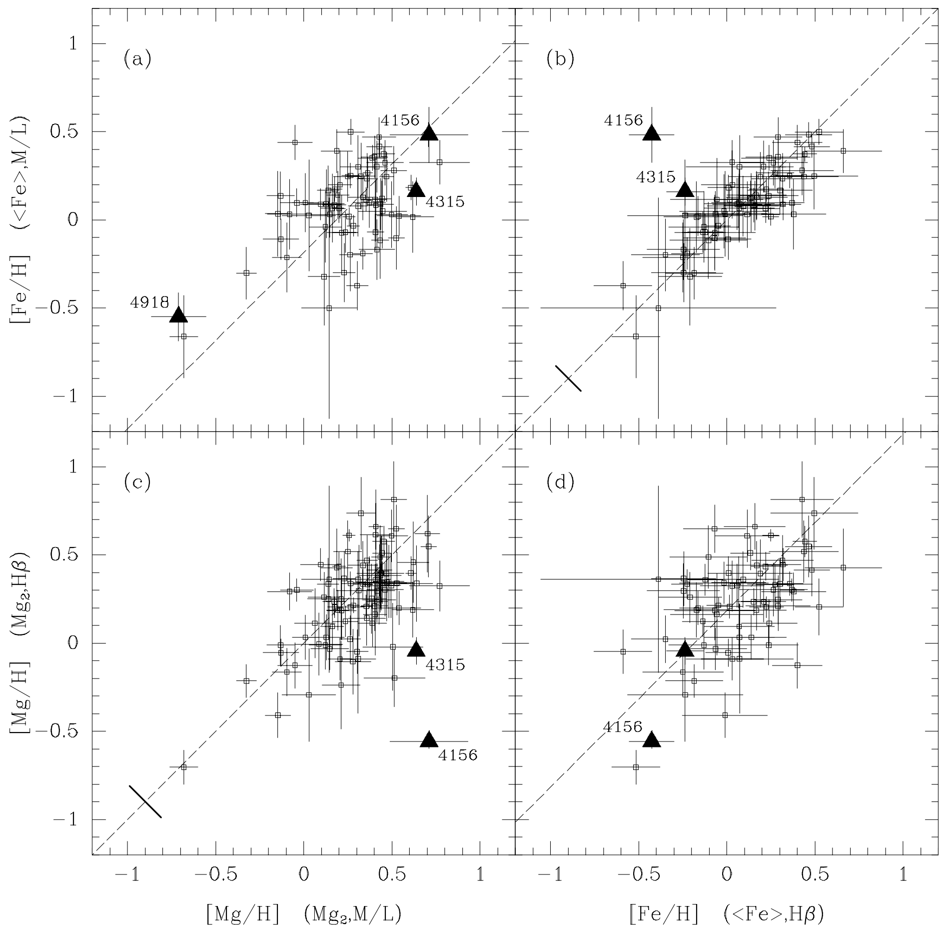

Figure 3. The two estimates of [Fe/H] and the two estimates of [Mg/H] versus each other. The parameters in parentheses refer to the diagram from which the ages were derived. Filled triangles – emission line galaxies. Dashed lines – one-to-one relations. The thick solid lines on panels (b) and (c) at (−0.9, −0.9) show the median measurement error relative to the one-to-one relation when the correlations of the measurement errors have been taken into account.

used then the two age estimates would have agreed. Thus, the requirement is as follows,

$$(0.91 - 0.18x) \log \mathrm{age}_{\mathrm{Mg_2,H\beta_G}} - 0.78 + 0.43x = 0.67 \log \mathrm{age}_{\mathrm{Mg_2},M/L} - 0.20 \qquad (6)$$

The slope x can then be derived as

$$x = \frac{0.67 \left(\log \mathrm{age}_{\mathrm{Mg_2},M/L} - \log \mathrm{age}_{\mathrm{Mg_2,H\beta_G}}\right)}{-0.18 \log \mathrm{age}_{\mathrm{Mg_2,H\beta_G}} + 0.43} + 1.35 \qquad (7)$$

The applied offset to $\log M/L$ results in a mean difference between the two age estimates of approximately zero when models with IMF slope $x = 1.35$ are used. Thus, equation (7) contains the implicit assumption that the mean slope is $x = 1.35$.

4.2 The [Mg/Fe] ratio

Fig. 3 shows the derived iron and magnesium abundances versus each other. There is good agreement between [Fe/H] derived from the <Fe>-Hβ_{G} diagram and those derived from the <Fe>-M/L diagram. The same is the case for the magnesium abundances. The iron abundances show slightly better agreement than the magnesium abundances. This is because [Fe/H] derived from the <Fe>-M/L diagram for most of the galaxies depends less on the M/L ratio than does [Mg/H] derived from the $\mathrm{Mg_2}$-M/L diagram, cf. Fig. 1(d) and (e). The variations in the fraction of dark matter (or the IMF slope) therefore affect the determination of $[\mathrm{Fe/H}]_{<\mathrm{Fe}>,M/L}$ less than it affects the determination of $[\mathrm{Mg/H}]_{\mathrm{Mg_2},M/L}$.

The two estimates of [Fe/H] are also shown versus the two estimates of [Mg/H], see Fig. 3(a) and (d). The scatter in these comparisons is due to real variations in the abundance ratio [Mg/Fe]. We derive two estimates of [Mg/Fe] as the difference between [Mg/H] and [Fe/H]. The determinations based on the Hβ_{G} index are not mixed with those based on the M/L ratio. Fig. 4 shows the two estimates versus each other. There is a very tight correlation and the scatter is comparable to the expected scatter due to measurement

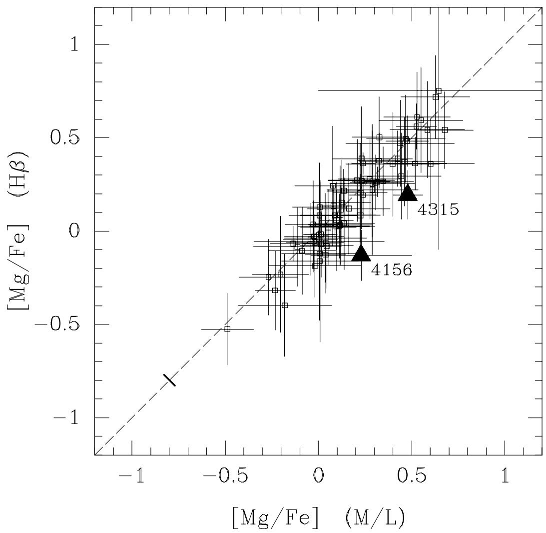

Figure 4. The two estimates of [Mg/Fe] versus each other. The age sensitive parameter used for the determination is given in parentheses. Filled triangles – emission line galaxies. Dashed line – one-to-one relation. The thick solid line at $(-0.8, -0.8)$ shows the median measurement error relative to the one-to-one relation when the correlation of the measurement errors has been taken into account.

errors. Thus, the variations in the fraction of dark matter (or in the IMF slope) do not significantly affect the abundance ratios [Mg/Fe] derived from the Mg_2-M/L diagram and the <Fe>-M/L diagram.

5 DISTRIBUTIONS OF THE DERIVED PARAMETERS

Fig. 5 shows the distributions of the ages, the abundances, and the dark matter fractions and the IMF slopes. The age determinations are based on Mg_2 as the metallicity sensitive parameter. The distribution of the dark matter fractions is shown for $f = 4$, cf. equation (4). The top axis on Fig. 5(b) gives the mass of the dark matter relative to the total mass for this choice of f. We chose $f = 4$, because this value is the smallest that results in positive dark matter masses for all the galaxies. In the following we primarily discuss the variations in the dark matter fraction and the correlations between the dark matter fraction and other parameters. The choice of f has no influence on this discussion.

We have tested if the distributions depend on whether the M/L ratio or the $H\beta_G$ index was used as the age sensitive parameter. Kolmogorov-Smirnov tests show that there are no significant differences in the distributions of the abundances [Mg/H] and [Fe/H] and the abundance ratio [Mg/Fe]. Thus, the determination of these distributions are not critically dependent on the choice of the age sensitive parameter.

A Kolmogorov-Smirnov test gives a probability of 5.5% that the two distributions of the ages shown on Fig. 5(a) are not different. However, if we limit the sample to those 90 galaxies that have available $H\beta_G$ the probability increases to 16.4%. We conclude that even though there is not a one-to-one relation between the ages derived from the two methods, cf. Section 4.1, the resulting distributions are not significantly different from each other.

Table 2 summarizes the median values of the derived mean ages, dark matter fractions, IMF slopes, and abundances together with the rms scatter, $\mathrm{rms_{obs}}$, and the typical measurement error, σ_{meas}. In order to judge if the rms scatter in the derived parameters reflects real variations in those parameters, we derive the difference $(\mathrm{rms_{obs}} - \sigma_{\mathrm{meas}})$ in units of the uncertainty on $\mathrm{rms_{obs}}$, see Table 2. All the parameters derived from the Mg_2 indices and the M/L ratios show real variations on the 5σ level or larger. When the $H\beta_G$ index is used as the age sensitive parameter the significance of the variations decreases to between 2σ and 4σ. This is due to the higher measurement uncertainty on the $H\beta_G$ index. Only for $[\mathrm{Mg/Fe}]_{H\beta_G}$ is the significance of the variations smaller than 2σ. However, since the two estimates of [Mg/Fe] are closely correlated (cf. Section 4.2) we conclude that the low significance of the real variations of $[\mathrm{Mg/Fe}]_{H\beta_G}$ is simply an affect of the uncertainty on the $H\beta_G$ index.

In summary, we find real variations in both the ages, the abundances and the abundance ratios. The dark matter fractions have variations significant on the 2σ level. If we assume that the fraction of dark matter does not vary, then variations in the slope of the IMF are significant on the 3σ level.

We quantify the variations by deriving the typical intrinsic rms scatter of each parameter as $\mathrm{rms_{int}} = (\mathrm{rms}^2_{\mathrm{obs}} - \sigma^2_{\mathrm{meas}})^{1/2}$. The intrinsic rms scatter $\mathrm{rms_{int}}$ does not depend significantly on whether the M/L ratio or the $H\beta_G$ index was used as the age sensitive parameter, cf. Table 2.

The intrinsic rms scatter of the ages is ≈ 0.2 dex, or about 50%. The oldest galaxies in the sample have mean ages of 15-20 Gyr, while the median age is about 5.0 Gyr. It is surprising that the median age is this low, and also that the sample contains a significant number of galaxies with mean ages below 3.5 Gyr. For the two different age estimates we find that 20-25% of the galaxies have mean ages younger than 3.5 Gyr. The derived ages are luminosity weighted mean ages of the stellar populations in the galaxies. The large variations in the derived mean ages and the presence of galaxies with very low mean ages show that many of these galaxies have experienced some star formation within the last 5 Gyr. While the absolute zero point of the mean ages is uncertain, the rms scatter of the age and the age differences do not depend on this zero point.

The median [Fe/H] is slightly above solar, while the median [Mg/H] is 0.25-0.3 dex above solar. The intrinsic rms scatter of both [Mg/H] and [Fe/H] is about 0.2 dex. The distributions are approximately Gaussian. The distribution of [Mg/Fe] is fairly flat, see Fig. 5, with a median value of 0.13 dex. 25 percent of the galaxies have [Mg/Fe] larger than 0.35 dex.

Further, our data show an intrinsic rms scatter in the dark matter fractions of ≈ 0.1 dex. Alternatively, the intrinsic rms scatter of the IMF slopes is ≈ 0.55.

We have tested whether the E and the S0 galaxies have different distributions of the derived ages, abundances, dark matter fraction and IMF slopes. For all the parameters except [Mg/Fe], Kolmogorov-Smirnov tests give probabilities of 42% or larger that the E and S0 galaxies were drawn from

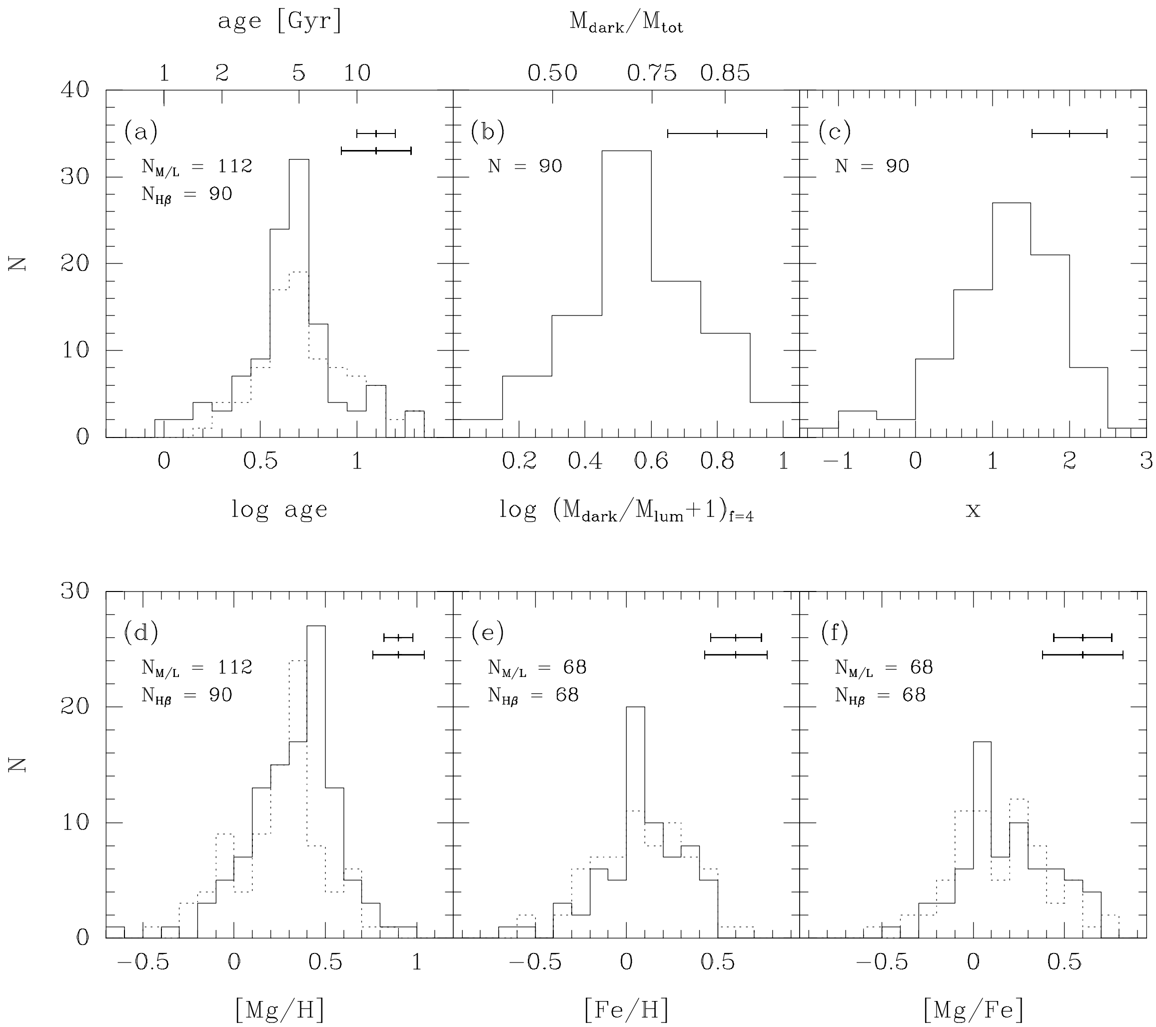

Figure 5. Distributions of (a) the ages using Mg_2 as the metallicity sensitive parameter, (b) the dark matter fractions, (c) the high-mass slopes x of the IMF, (d) [Mg/H], (e) [Fe/H], and (f) [Mg/Fe]. On panels (a) and (d)-(f) the solid lines are histograms of the parameters derived using the M/L ratio as the age sensitive parameter. The dotted lines are histograms of the parameters derived using $H\beta_G$ as the age sensitive parameter. The dark matter fractions and the slopes of the IMF are derived as described in Section 4.1. The number of galaxies included in each histogram is given on the panels. The error bars show the one sigma uncertainty. On panels (a), (d), (e) and (f) the top error bar refers to parameters derived using the M/L ratio as the age sensitive parameter, while the bottom error bar refers to parameters derived using $H\beta_G$ as the age sensitive parameter.

the same parent distribution. For [Mg/Fe], we find probabilities of 0.3% and 0.9% for parameters based on the M/L ratios and the $H\beta_G$ indices, respectively. Part of the difference between the E and S0 galaxies is caused by the six brightest galaxies. If we exclude those galaxies, the probabilities increase to 2.4% and 6%, respectively. The S0 galaxies have on average lower [Mg/Fe] than do the E galaxies. The median [Mg/Fe] values (based on $H\beta_G$) are 0.267 and 0.040 for the E and S0 galaxies, respectively. However, as we will show in Sections 7 and 8, the E and S0 galaxies follow the same relations between ages, abundances and velocity dispersions, and they also follow the same empirical scaling relations.

Faber et al. (1995) found for a sample of mostly field galaxies with data from González (1993) that the mean metallicity [M/H] was $\approx$ 0.3 dex and showed little variation. The ages of the galaxies in that sample vary between 2 Gyr and 12 Gyr. Judging from Figure 2 in Faber et al., the median age is about 5 Gyr. We note, that Kuntschner & Davies [1998] show the same data and models to give a median age of about 8 Gyr, see their Figure 1b. The study by Faber et al. was based on $H\beta$ and the geometrical mean of the magnesium index Mg*b* and the <Fe> index, called [MgFe] by these authors. Thus, the variations in [Mg/Fe] were not taken into account.

Kuntschner & Davies (1998) used the same technique to derive mean ages and metallicities for a sample of E and S0 galaxies in the Fornax cluster. [M/H] for this sample is between ≈ -0.25 dex and ≈ 0.5 dex. The elliptical galax-

Table 2. Median values and rms scatter of derived parameters

Parameter	N	Median	rms_{obs}	σ_{meas}	Δ	rms_{int}
log age (Mg_2,M/L)	112	0.66	0.244±0.023	0.094	6.5	0.225
log age (Mg_2,M/L)[a]	90	0.67	0.223±0.024	0.101	5.2	0.199
log age (Mg_2,M/L)[b]	68	0.68	0.223±0.027	0.087	5.0	0.205
log age (Mg_2,$H\beta_G$)	90	0.72	0.264±0.028	0.206	2.1	0.166
log age (Mg_2,$H\beta_G$)[b]	68	0.70	0.260±0.031	0.183	2.4	0.184
$\log\left(\frac{M_{\rm dark}}{M_{\rm lum}}+1\right)_{\rm f=4}$	90	0.55	0.201±0.021	0.152	2.3	0.131
x (IMF slope)	90	1.18	0.803±0.085	0.507	3.5	0.624
[Mg/H] (Mg_2,M/L)	112	0.36	0.240±0.023	0.090	6.6	0.223
[Mg/H] (Mg_2,M/L)[a]	90	0.33	0.233±0.025	0.081	6.2	0.219
[Mg/H] (Mg_2,M/L)[b]	68	0.29	0.242±0.029	0.074	5.7	0.230
[Mg/H] (Mg_2,$H\beta_G$)	90	0.30	0.262±0.028	0.144	4.3	0.219
[Mg/H] (Mg_2,$H\beta_G$)[b]	68	0.29	0.272±0.033	0.130	4.3	0.238
[Fe/H] (<Fe>,M/L)	68	0.09	0.232±0.028	0.138	3.3	0.187
[Fe/H] (<Fe>,$H\beta_G$)	68	0.08	0.260±0.032	0.174	2.7	0.194
[Mg/Fe] (M/L)	68	0.13	0.247±0.030	0.158	3.0	0.190
[Mg/Fe] ($H\beta_G$)	68	0.13	0.268±0.033	0.216	1.6	0.160

Note – The emission line galaxies have been omitted. For the ages and the metallicities, the age and metallicity sensitive parameters used for the determinations are given in parentheses after the parameter name. The determinations of fraction of dark matter and the slope of the IMF are described in Section 4.1. For [Mg/Fe] the age sensitive parameter used for the determination is given in parentheses. [a] Galaxies with available $H\beta_G$. [b] Galaxies with available $H\beta_G$ and <Fe>. "Δ" gives the difference $rms_{obs} - \sigma_{meas}$ in units of the uncertainty on rms_{obs}.

ies have mean ages between 5 Gyr and 12 Gyr, the median ages is about 8 Gyr. Some of the S0 galaxies have significantly lower mean ages. The large scatter in [M/H] found by Kuntschner & Davies compared to Faber et al. (1995) may be due to a larger luminosity range of the sample studied by Kuntschner & Davies.

Our results are in general agreement with both of these studies in terms of the variations detected in both the mean ages and the mean metallicities. We find a median age which is lower than found by Kuntschner & Davies, and also lower than found by these authors' analysis of the data from González (1993). Faber et al. and Kuntschner & Davies used the stellar population models from Worthey (1994), while we use the models from Vazdekis et al. (1996). There are three sources of differences related to the stellar populations models. (1) The difference in the assumed IMF; Worthey (1994) uses a Salpeter IMF, while the models we use from Vazdekis et al. assume a Scalo-like IMF. (2) The difference in the isochrones; Worthey (1994) uses the VandenBerg isochrones (VandenBerg 1985; VandenBerg & Bell 1985; VandenBerg & Laskarides 1987) and the Revised Yale Isochrones (Green et al. 1987), while Vazdekis et al. use isochrones from the Padova group (Bertelli et al. 1994). (3) Faber et al. and Kuntschner & Davies derive ages and metallicities from the [MgFe]-Hβ diagram, while the zero point for our age and metallicity determinations is based on the <Fe>-$H\beta_G$ diagram. (The difference in the definition of the Hβ index has no significant effect.)

We tested the effect of these difference by deriving the ages and metallicities for all the methods for a hypothetical galaxy with the all indices equal to the mean values of our sample. By comparing models from Vazdekis et al. with a Scalo-like IMF to those with a Salpeter IMF we find that the difference in IMF has a negligible effect on ages and metallicities derived from the <Fe>-$H\beta_G$ diagram and from the [MgFe]-Hβ diagram. The differences in both age and [M/H] are less than 0.01 dex.

Using the <Fe>-$H\beta_G$ diagram, we compared ages and metallicities derived using Worthey's models and the models from Vazdekis et al. (with a Scalo-like IMF), respectively. The models from Worthey result in ages that are ≈0.13 dex older than those derived using the models Vazdekis et al. The resulting metallicities are 0.06 lower for the models from Worthey. These differences due to the choice of the isochrones were also noted by Worthey et al. (1995).

Finally, we compared ages and metallicities derived from the <Fe>-$H\beta_G$ diagram with those derived using the [MgFe]-Hβ diagram. Ages derived from the <Fe>-$H\beta_G$ diagram are ≈0.1 dex lower than those derived from the [MgFe]-Hβ diagram, while metallicities are ≈0.15 dex higher. This is the case for both Worthey's models and the models from Vazdekis et al.

If we had used the [MgFe]-Hβ diagram and Worthey's models, the resulting ages for our sample would have a median value of ≈ 4.6 Gyr. This is significantly younger than the median ages found by Kuntschner & Davies. We therefore speculate that our sample of Coma cluster galaxies have experienced episodes of more recent star formation than the galaxies studied by Kuntschner & Davies.

6 PROPERTIES AS FUNCTIONS OF MASS, LUMINOSITY AND VELOCITY DISPERSION

In this section we study how the derived mean ages, the dark matter fractions (or the IMF slopes) and the abundances vary with the masses, the luminosities, and the central velocity dispersions of the galaxies. We also briefly discuss the possible projection effects on the derived parameters. The ages and abundances derived for the three galaxies with emission lines are highly affected by the emission lines. Therefore these galaxies were omitted in the correlation tests and the determination of the linear relations presented in the following.

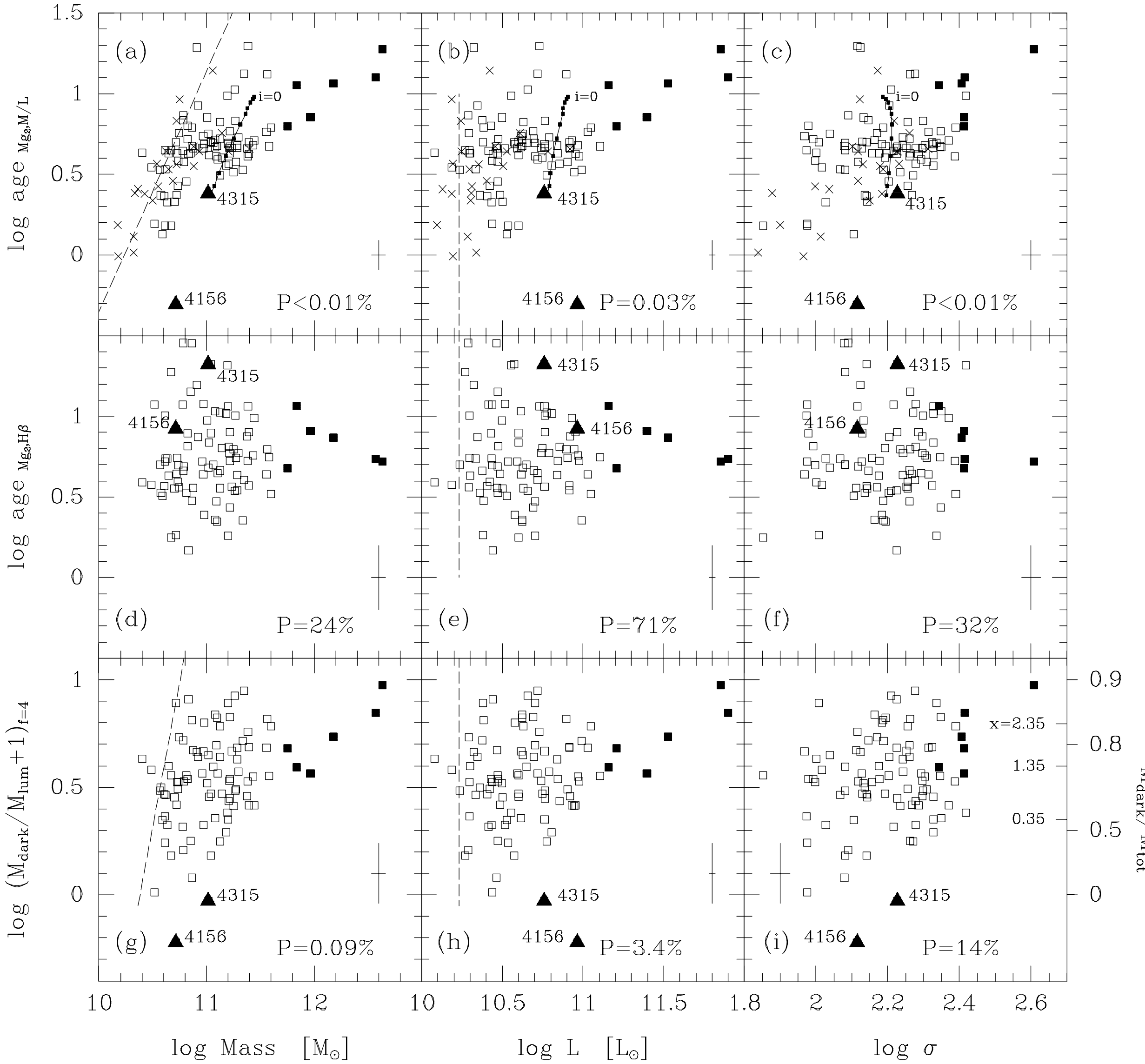

Figure 6. The derived ages and the dark matter fractions versus the masses, the luminosities and the velocity dispersions of the galaxies. The determinations are based on Mg_2, $\mathrm{H}\beta_\mathrm{G}$ and the M/L ratio. Boxes – galaxies with all three parameters derived; crosses – galaxies without $\mathrm{H}\beta_\mathrm{G}$ measurement and therefore without determination of the fraction of dark matter. Filled triangles – galaxies with emission lines. Filled boxes – galaxies brighter than $M_{\mathrm{r_T}} = -23^{\mathrm{m}}1$. Typical error bars are given on the panels. The dashed lines show the approximate completeness limit of the sample. The fraction of dark matter is shown for $f = 4$, cf. equation (3). This equivalent to assuming that the mean fraction of dark matter in the sample galaxies is 75%. The right axis on panel (i) shows the dark matter mass relative to the total mass for this value of f. The axis also shows the approximate IMF slope x, under the assumption that the dark matter fraction is constant. The possible projection effects for a model with $L_\mathrm{D}/L_\mathrm{tot} = 0.4$ are shown in panels (a)-(c) as small filled boxes connected by a solid line. The models are evenly distributed in cosine of the inclination i, with i between zero (labeled on panels) and 90 degrees. Inclination zero (face-on) leads to the largest derived age.

6.1 Model predictions of the projection effects

The photometric parameters and velocity dispersions are subject to projection effects. Therefore, also the masses, the M/L ratios, and the ages and abundances derived using the M/L ratio as the age sensitive parameter will be subject to projection effects. We have estimated the projection effects based on the same kind of models used by JFK96 to estimate the projection effects for the FP. The photometric models are axisymmetric and consist of an exponential disk and a bulge with an $R^{1/4}$ luminosity profile. Both components are oblate. The intrinsic ellipticities were 0.3 and 0.85 for the bulge and the disk, respectively. The model images were convolved with the seeing, and then processed the same way as the observations in order to derive the photometric parameters. The kinematic models were made under the assumption that the distribution function is a function only of the en-

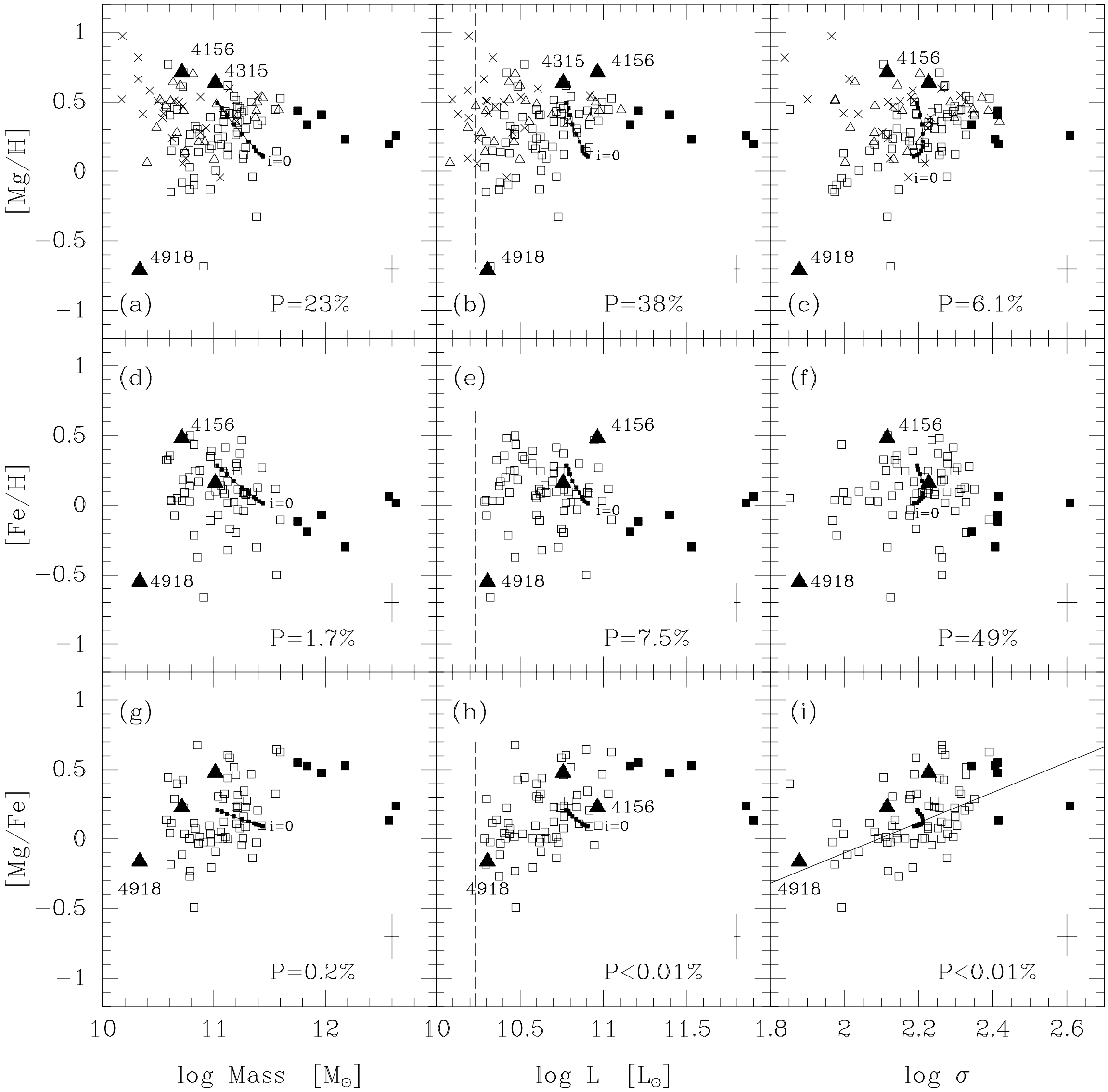

Figure 7. The derived abundances [Mg/H] and [Fe/H] as well as the abundance ratio [Mg/Fe] versus the masses, the luminosities and the velocity dispersions of the galaxies. The determinations of the abundances are based on Mg_2, <Fe> and the M/L ratio. Boxes – galaxies with all three parameters derived; triangles – galaxies with available $\mathrm{H}\beta_\mathrm{G}$ but no <Fe> measurement; crosses – galaxies without <Fe> and $\mathrm{H}\beta_\mathrm{G}$ measurements. Filled triangles – galaxies with emission lines. Filled boxes – galaxies brighter than $M_{\mathrm{r_T}} = -23\overset{\mathrm{m}}{.}1$. Typical error bars are given on the panels. The dashed lines show the approximate completeness limit of the sample. The possible projection effects for a model with $L_\mathrm{D}/L_\mathrm{tot} = 0.4$ is shown as small filled boxes connected by a solid line. The models are evenly distributed in cosine of the inclination i, with i between zero (labeled on panels) and 90 degrees. Inclination zero (face-on) leads to the smallest derived [Mg/H], [Fe/H] and [Mg/Fe]. The solid line on panel (i) is the relation given in equation (8).

ergy E and the angular momentum L_z around the z-axis. Models were made for relative disk luminosities $L_\mathrm{D}/L_\mathrm{tot}$ between zero and one and inclinations between zero (face-on) and 90 degrees (edge-on). Small projection effects in the indices Mg_2 and <Fe> are expected due to the combination of the radial gradients in the indices and how the fraction of the galaxy sampled by a given aperture size changes as a function of the inclination. These small effects can safely be ignored and we assume that the Mg_2 and <Fe> are not affected by the projection effects. For a given $L_\mathrm{D}/L_\mathrm{tot}$, we derive Mg_2 and <Fe> from the mean velocity dispersion of models with random spatial orientation. We assume that the models follow the relations between the line indices and the velocity dispersion derived by J97.

The models and the projection effects are discussed in more detail in Milvang-Jensen & Jørgensen (1998, in prep.). In this paper we use a model with $L_\mathrm{D}/L_\mathrm{tot} = 0.4$ as a representative model. Models with smaller $L_\mathrm{D}/L_\mathrm{tot}$ have smaller projection effects. The models are fairly simple and we will use them only to illustrate the possible projection effects.

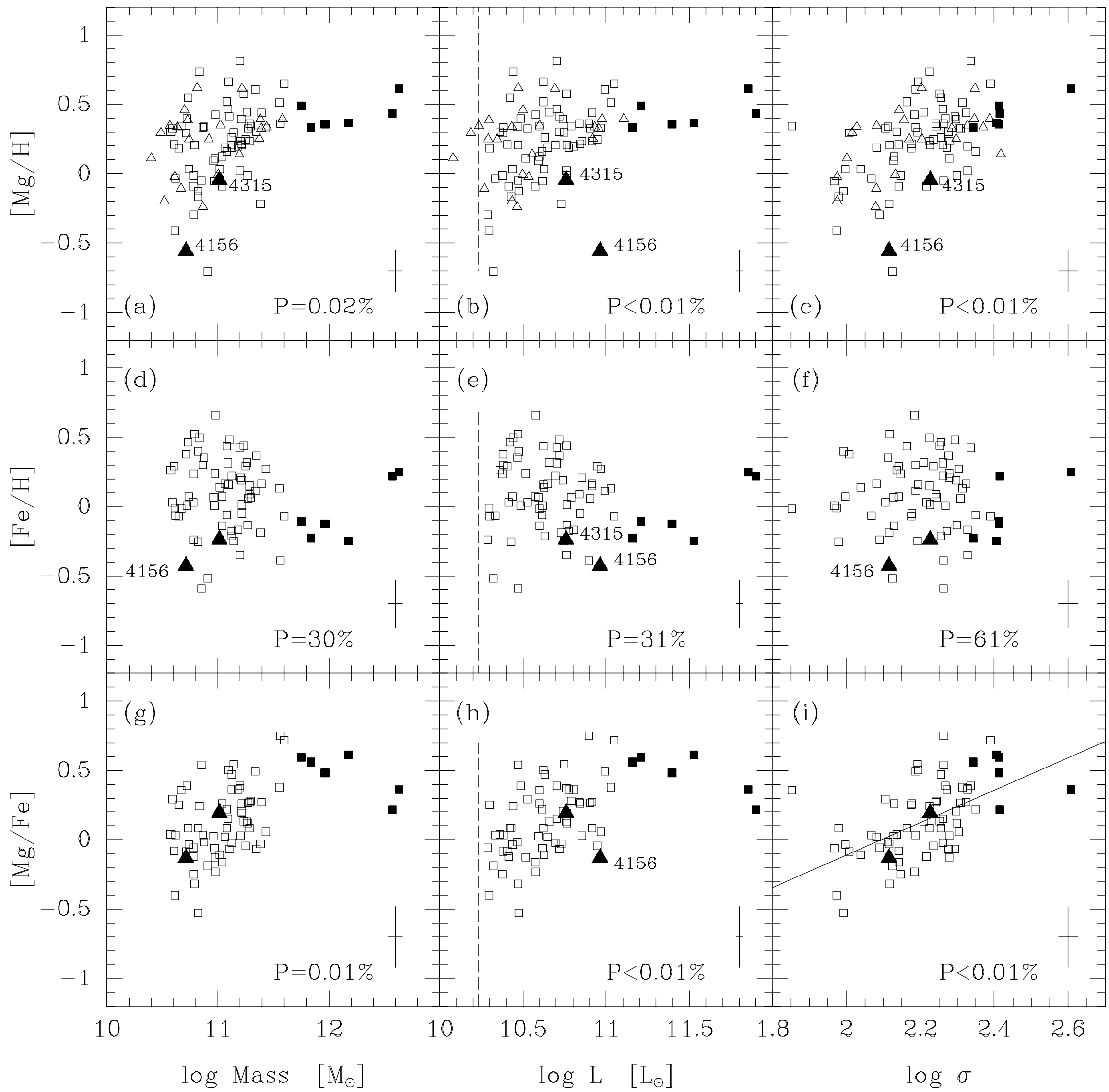

Figure 8. The derived abundances [Mg/H] and [Fe/H] as well as the abundance ratio [Mg/Fe] versus the masses, luminosities and velocity dispersions of the galaxies. The determinations of the abundances are based on Mg_2, <Fe> and $H\beta_G$. Boxes – galaxies with all three parameters derived; triangles – galaxies with no <Fe> measurement. Filled triangles – galaxies with emission lines. Filled boxes – galaxies brighter than $M_{r_T} = -23.^{m}1$. Typical error bars are given on the panels. The dashed lines show the approximate completeness limit of the sample. The solid line on panel (i) is the relation given in equation (9).

6.2 The ages and the fraction of dark matter

Fig. 6 shows the two age estimates and the dark matter fractions as a function of the masses, the luminosities and the velocity dispersions of the galaxies. The ages and the dark matter fractions are derived from the Mg_2-$H\beta_G$ diagram and the Mg_2-M/L diagram. Using the <Fe> index instead of the Mg_2 index leads to the same conclusions as those discussed in the following. The right axis on Fig. 6(i) shows the dark matter fraction as well as the IMF slope if we assume a constant fraction of dark matter. In the following, where the dark matter fractions are discussed we could alternatively use the interpretation that the IMF slope varies and the dark matter fraction is constant.

The ages, $\mathrm{age}_{Mg_2,H\beta_G}$, based on the Mg_2-$H\beta_G$ diagram are uncorrelated with the galaxy masses, luminosities and velocity dispersions, cf. Fig. 6(d)-(f). Spearman rank order tests give probabilities P=24% or larger that there are no correlations between these parameters. The ages based on the M/L ratio show correlations with all three tested parameters. Spearman rank order tests give probabilities P=0.03% or smaller that there are no correlations. The possible projection effects for a model with $L_D/L_{tot} = 0.4$ are shown on Fig. 6(a)-(c). The face-on orientation of the model results in a higher derived age than the edge-on orientation. The projection effects are almost perpendicular to the correlations and would weaken the correlations. Thus, the correlations cannot be caused by the projection effects. Most likely the correlations are due to underlying correlations between the fraction of dark matter and the masses, the luminosities and the velocity dispersions of the galaxies. Because $\mathrm{age}_{\mathrm{Mg_2,H\beta_G}}$ is not affected by the variations in the dark matter fractions, we regard $\mathrm{age}_{\mathrm{Mg_2,H\beta_G}}$ as a more reliable determination of the age than the age derived from the $\mathrm{Mg_2}$-M/L diagram.

A Spearman rank order test gives a probability of P=0.09% that there is no correlation between the dark matter fractions and the masses of the galaxies. The fraction of dark matter is also weakly correlated with the luminosities of the galaxies; a Spearman rank order test gives a probability of 3.4% that there is no correlation. We do not detect a significant correlation between the dark matter fractions and the velocity dispersions; a Spearman rank order test gives a probability of 14% that there is no correlation. The uncertainties on the estimated dark matter fractions are rather large and more accurate measurements, especially of the $\mathrm{H\beta_G}$ indices, are needed to study these correlations in further detail.

The six most massive and luminous galaxies ($M_{\mathrm{r_T}}$ brighter than $-23\overset{\mathrm{m}}{.}1$) in the sample show less variation in their ages and dark matter fractions than do the less massive galaxies. The rms variations of $\log \mathrm{age}_{\mathrm{Mg_2,H\beta_G}}$ is 0.15 and 0.26 for the massive and the less massive galaxies, respectively. Also Worthey (1996) notes that the largest E galaxies seem more homogeneous in their ages than the smaller E galaxies. A larger sample of very luminous E galaxies is required in order to conclude if this is a common property for such luminous galaxies.

6.3 The metallicities and the abundance ratios

In Fig. 7 and Fig. 8, the derived metallicities and the abundance ratios [Mg/Fe] are shown versus the masses, luminosities and velocity dispersions of the galaxies. The determinations shown on Fig. 7 are based on the M/L ratios and the line indices $\mathrm{Mg_2}$ and <Fe>, while the determinations in Fig. 8 were derived from $\mathrm{H\beta_G}$, $\mathrm{Mg_2}$ and <Fe>.

The six most massive galaxies in the sample show less variation in [Mg/H] and [Fe/H] than do the less massive galaxies. Thus, these galaxies are rather homogeneous in both their ages and their metal content.

We have used Spearman rank order tests to test for correlations between the abundances and the masses, the luminosities and the velocity dispersions of the galaxies. The probability that there is no correlation between the tested parameters is given on each panel of Figs. 7 and 8. No significant correlations are found for [Mg/H] derived from the $\mathrm{Mg_2}$-M/L diagram, while [Mg/H] derived from the $\mathrm{Mg_2}$-$\mathrm{H\beta_G}$ diagram show strong correlations with all three tested parameters. The difference is partly due to the difference in the samples used for the tests, since $\mathrm{H\beta_G}$ is not available for all the galaxies. Limiting the sample to those galaxies for which $\mathrm{H\beta_G}$ is available, we find probabilities of P=59%, P=1.5% and P=0.1% that $[\mathrm{Mg/H}]_{\mathrm{Mg_2},M/L}$ is uncorrelated with the masses, the luminosities and the velocity dispersions, respectively. Projection effects may also work to weaken the correlations involving $[\mathrm{Mg/H}]_{\mathrm{Mg_2},M/L}$, see Fig. 7(a)-(c). Finally, variations in the fraction of dark matter may affect

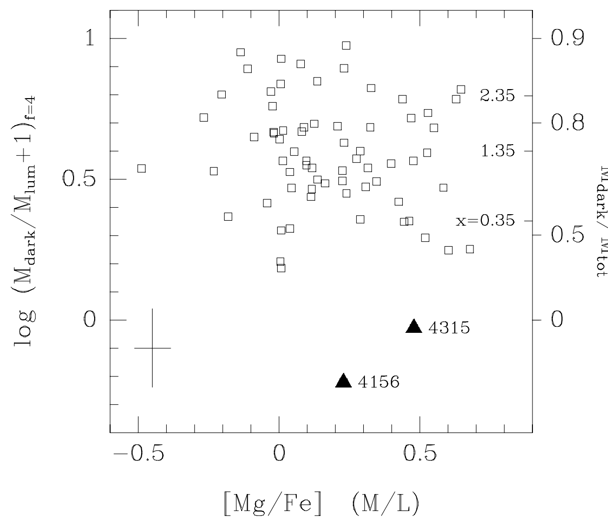

Figure 9. The dark matter fraction as a function of [Mg/Fe]. The right axis also shows the IMF slope x under the assumption that the dark matter fraction is constant. Solid symbols – galaxies with emission lines. Typical error bars are given on the figure. The two parameters are not significantly correlated.

$[\mathrm{Mg/H}]_{\mathrm{Mg_2},M/L}$. It would be valuable to measure $\mathrm{H\beta_G}$ for the full sample in order to ensure that the correlations found for $[\mathrm{Mg/H}]_{\mathrm{Mg_2,H\beta_G}}$ are not due to selection effects.

The iron abundance, [Fe/H], is in general uncorrelated with the masses, the luminosities and the velocity dispersions. We do find a correlation between $[\mathrm{Fe/H}]_{<\mathrm{Fe}>,M/L}$ and the masses of the galaxies, see Fig. 8(d). This correlation may be partly due to the projection effects, which are expected to strengthen the correlation.

The strongest correlations are found between the abundance ratio [Mg/Fe] and the velocity dispersions and the luminosities. For both determinations of [Mg/Fe] Spearman rank order tests give probabilities of P<0.01% that they are uncorrelated with the the velocity dispersions and the luminosities. There is also a significant correlation between [Mg/Fe] and the masses of the galaxies; Spearman rank order tests give a probability of no correlation of 0.2% and 0.01% for [Mg/Fe] based on the M/L ratio and the $\mathrm{H\beta_G}$ index, respectively.

The abundance ratio [Mg/Fe] increases with the mass, the luminosity and the velocity dispersion. This effect was also found by Worthey et al. (1992) who estimated the most luminous galaxies to have [Mg/Fe] about 0.3 dex above solar. J97 found [Mg/Fe] to increase with 0.3-0.4 dex over 0.4 dex in $\log \sigma$. For [Mg/Fe] based on the M/L ratios, we find

$$[\mathrm{Mg/Fe}] = (1.09 \pm 0.34) \log \sigma - 2.28 \quad (8)$$

with an rms scatter of 0.22 in [Mg/Fe]. The sum of the absolute residuals in [Mg/Fe] were minimized, and the uncertainty of the coefficient derived with a boot-strap method. The relation for [Mg/Fe] based on the $\mathrm{H\beta_G}$ index has a slightly steeper slope. We find

$$[\mathrm{Mg/Fe}] = (1.17 \pm 0.35) \log \sigma - 2.45 \quad (9)$$

with an rms scatter of 0.23. The relations are shown on Fig. 7(i) and Fig. 8(i), respectively. The relations are in agree-

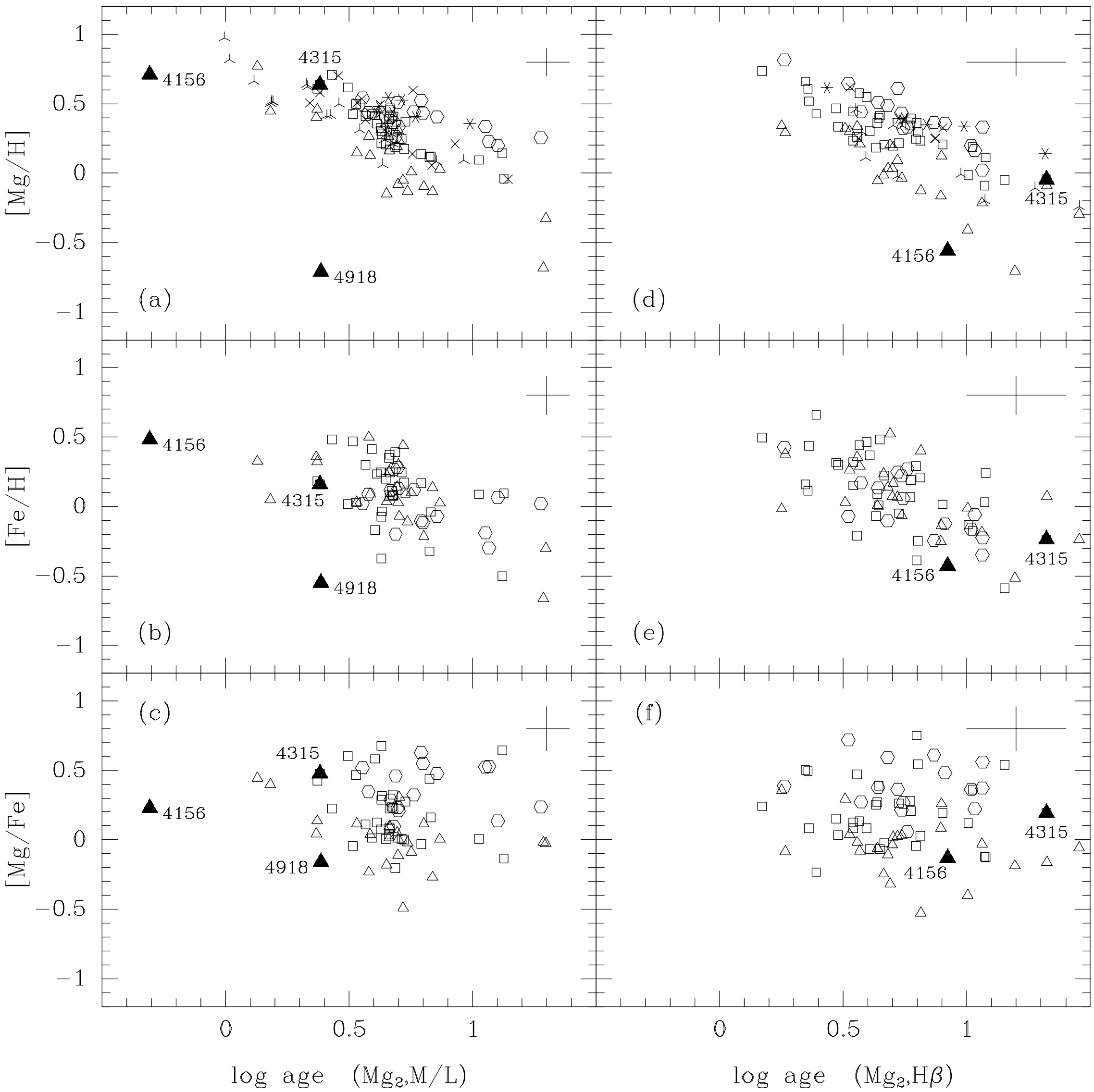

Figure 10. The mean abundances, [Mg/H] and [Fe/H], and the abundance ratios [Mg/Fe] versus the mean ages. Age and abundance determinations based on the M/L ratio as the age sensitive parameter are shown on panels (a)-(c). Age and abundance determinations based on the $H\beta_G$ as the age sensitive parameter are shown on panels (d)-(f). Typical error bars are given on the panels. Open symbols – galaxies with all parameters determined; skeletal symbols – galaxies with no measurement of <Fe>. There are more galaxies included in panel (a) than in panel (d), because not all galaxies have measurements of $H\beta_G$. The number of vertices on the symbols reflect the velocity dispersion as follows; three vertices – $\log\sigma$ in the interval 1.8–2.15; four vertices – $\log\sigma$ in the interval 2.15–2.3; six vertices – $\log\sigma$ in the interval 2.3–2.65. Solid triangles – galaxies with emission lines.

ment with the results from J97 and Worthey et al. (1992). Because [Fe/H] is uncorrelated with the velocity dispersion, the correlations in equations 8 and 9 are mostly due to the correlation between [Mg/H] and the velocity dispersion, which in turn to some extent represents the Mg_2-σ relation. However, the slope of the Mg_2-σ is best explained as due to variations in both [Mg/H] and the ages. We will discuss this in detail in Section 8.1.

Fig. 9 shows the abundance ratio [Mg/Fe] as a function of the dark matter fraction (or the IMF slope). It has been suggested that the above solar [Mg/Fe] values for the most massive galaxies are caused by a shallow IMF, maybe during a period of strong star formation early in the history of these galaxies (e.g., Vazdekis et al. 1996). Such a period of star formation presumably leaves behind a large amount of stellar remnants, that should then lead to a larger fraction of dark matter. However, we find that [Mg/Fe] and the dark matter fraction are not correlated. If we assume a constant

Table 3. Age-metallicity-velocity dispersion relations

Rel.	Basis	Technique	N	Relation	rms
1	$\mathrm{H}\beta_\mathrm{G}$	$\Sigma\Delta y^2$	90	$[\mathrm{Mg/H}] = -0.73 \log \mathrm{age} + 1.08 \log \sigma - 1.60$	0.12
				$\pm 0.05 \qquad \pm 0.10$	
2	$\mathrm{H}\beta_\mathrm{G}$	$\Sigma\Delta y^2$	68[a]	$[\mathrm{Mg/H}] = -0.80 \log \mathrm{age} + 1.21 \log \sigma - 1.86$	0.11
				$\pm 0.05 \qquad \pm 0.11$	
3	$\mathrm{H}\beta_\mathrm{G}$	$\Sigma\lvert\Delta y\rvert$	90	$[\mathrm{Mg/H}] = -0.66 \log \mathrm{age} + 1.05 \log \sigma - 1.58$	0.12
				$\pm 0.07 \qquad \pm 0.12$	
4	$\mathrm{H}\beta_\mathrm{G}$	$\Sigma\lvert\Delta y\rvert$	68[a]	$[\mathrm{Mg/H}] = -0.84 \log \mathrm{age} + 1.19 \log \sigma - 1.77$	0.11
				$\pm 0.10 \qquad \pm 0.12$	
5	$\mathrm{H}\beta_\mathrm{G}$	$\Sigma\Delta y^2$	68	$[\mathrm{Fe/H}] = -0.62 \log \mathrm{age} + 0.06 \log \sigma + 0.41$	0.21
				$\pm 0.10 \qquad \pm 0.19$	
6	$\mathrm{H}\beta_\mathrm{G}$	$\Sigma\lvert\Delta y\rvert$	68	$[\mathrm{Fe/H}] = -0.75 \log \mathrm{age} + 0.07 \log \sigma + 0.45$	0.21
				$\pm 0.13 \qquad \pm 0.23$	
7	$\mathrm{H}\beta_\mathrm{G}$	$\Sigma\Delta y^2$	68	$[\mathrm{Mg/Fe}] = -0.17 \log \mathrm{age} + 1.15 \log \sigma - 2.27$	0.23
				$\pm 0.11 \qquad \pm 0.21$	
8	$\mathrm{H}\beta_\mathrm{G}$	$\Sigma\lvert\Delta y\rvert$	68	$[\mathrm{Mg/Fe}] = -0.12 \log \mathrm{age} + 1.16 \log \sigma - 2.35$	0.23
				$\pm 0.11 \qquad \pm 0.29$	
9	M/L	$\Sigma\Delta y^2$	112	$[\mathrm{Mg/H}] = -1.00 \log \mathrm{age} + 1.12 \log \sigma - 1.48$	0.11
				$\pm 0.04 \qquad \pm 0.08$	
10	M/L	$\Sigma\Delta y^2$	68[a]	$[\mathrm{Mg/H}] = -0.93 \log \mathrm{age} + 1.31 \log \sigma - 1.99$	0.10
				$\pm 0.05 \qquad \pm 0.09$	
11	M/L	$\Sigma\lvert\Delta y\rvert$	112	$[\mathrm{Mg/H}] = -0.93 \log \mathrm{age} + 1.06 \log \sigma - 1.38$	0.11
				$\pm 0.07 \qquad \pm 0.14$	
12	M/L	$\Sigma\lvert\Delta y\rvert$	68[a]	$[\mathrm{Mg/H}] = -0.82 \log \mathrm{age} + 1.22 \log \sigma - 1.85$	0.11
				$\pm 0.07 \qquad \pm 0.10$	
13	M/L	$\Sigma\Delta y^2$	68	$[\mathrm{Fe/H}] = -0.62 \log \mathrm{age} + 0.24 \log \sigma - 0.01$	0.20
				$\pm 0.11 \qquad \pm 0.18$	
14	M/L	$\Sigma\lvert\Delta y\rvert$	68	$[\mathrm{Fe/H}] = -0.46 \log \mathrm{age} + 0.33 \log \sigma - 0.30$	0.20
				$\pm 0.21 \qquad \pm 0.21$	
15	M/L	$\Sigma\Delta y^2$	68	$[\mathrm{Mg/Fe}] = -0.31 \log \mathrm{age} + 1.07 \log \sigma - 1.97$	0.21
				$\pm 0.12 \qquad \pm 0.20$	
16	M/L	$\Sigma\lvert\Delta y\rvert$	68	$[\mathrm{Mg/Fe}] = -0.31 \log \mathrm{age} + 0.76 \log \sigma - 1.31$	0.21
				$\pm 0.19 \qquad \pm 0.26$	

Notes – Basis: the age sensitive parameter used for deriving ages and abundances. Techniques: $\Sigma\Delta y^2$ – least squares fit. $\Sigma|\Delta y|$ – the sum of the absolute residuals has been minimized and the uncertainties derived with a boot-strap method. [a] Only galaxies with available <Fe> are included; these galaxies have all parameters available.

dark matter fraction, then Fig. 9 shows that [Mg/Fe] is uncorrelated with the slope of the IMF. The derived IMF slope should be understood as the current slope of the luminosity weighted stellar mass function.

7 THE AGE-METALLICITY-VELOCITY DISPERSION RELATION

Fig. 10 shows the abundances versus the ages. The ages and the abundances [Mg/H] and [Fe/H] are strongly anti-correlated, while [Mg/Fe] is not significantly correlated with the ages. The magnesium abundance, [Mg/H], also depends on the velocity dispersion. For a given age, galaxies with higher velocity dispersions have higher metallicities, cf. Figs. 10(a) and 10(d), see also Fig. 8(c). The correlation between [Mg/H] and the velocity dispersion to some extent represents the Mg_2-σ relation, though the slope of the Mg_2-σ relation is best explained as due to variations in both [Mg/H] and the ages (cf. Section 8.1).

We have derived linear relations between the abundances, the ages and the velocity dispersions. Also relations between the abundance ratio [Mg/Fe], the ages and the velocity dispersions were determined. The relations are summarized in Table 3. Relations involving [Mg/H] were also derived for the sub-sample of 68 galaxies for which all spectroscopic parameters are available. The differences between the coefficients for the relations for the sub-sample and those for the larger samples are no larger than 1.6 times the uncertainties on the differences. Thus, the incompleteness of the sub-sample with all available spectroscopic parameters is not expected to affect the following discussion and results.

Further, we divided the sample in E and S0 galaxies and fitted the relations to each of the classes separately. We find that the relations for the E and S0 galaxies are not significantly different from each other. The age-[Mg/H]-σ relations show the largest differences between the coefficients for E and S0 galaxies, 1.6 times the uncertainties on the differences. Also, the zero points for the E and S0 galaxies relative to their common relations as given in Table 3 are not significantly different. Except for the age-[Mg/H]-σ relations, their differences are all less than the uncertainties on the differences. The age-[Mg/H]-σ relations show differences of about twice the uncertainties on the differences. Since there are no strong indications of the E and S0 galaxies following different relations, we will in the following treat the galaxies as one class of galaxies.

Relations are given for ages and abundances based on the M/L ratio as the age sensitive parameter as well as based on the Hβ_G index as the age sensitive parameter. The differences between the two sets of relations are due to the correlation between the velocity dispersions and the ages based on the M/L ratios. If our interpretation of the differences in the two age estimates is correct, then the ages are best determined using Hβ_G as the age sensitive parameter. Thus, relations (9)-(16) in Table 3 must be preferred as the best determinations of the relations between the ages, the abundances and the velocity dispersions.

For [Fe/H], the velocity dispersion term in the relations is not significant. Thus, the iron abundance of a galaxy scales with the mean age of the stellar populations in the galaxy but does not depend on the velocity dispersion of the galaxy.

The relations for [Mg/H] have significant terms for both the age and the velocity dispersion. The derived relations are in agreement with the age-metal relation presented by Worthey et al. (1995). These authors used the C4668 index rather than Mg_2. C4668 is correlated with Mg_2, though the relation has substantial intrinsic scatter (cf. J97). Therefore, we do not expect a very close agreement between the relations derived here and the results by Worthey et al. (1995). The significance of both the age and the velocity dispersion term may indicate that the magnesium abundance increases with later episodes of star formation but that part of the magnesium enrichment is determined by the velocity dispersion of the galaxies.

The relations for the abundance ratio [Mg/Fe] have no significant age term, while [Mg/Fe] increases with the velocity dispersion. The coefficient for the velocity dispersion term is in qualitative agreement with the results from Worthey et al. (1992) and from J97, see Section 6.3. The increase in [Mg/Fe] with the velocity dispersion can also be deduced directly from the difference in the slopes of the Mg_2-σ relation and the <Fe>-σ relation (e.g., Fisher et al. 1995, J97, Trager et al. 1998). Because Mg_2 and log <Fe> are expected to change in a similar way with age (cf., Table 1), the difference in the slope of the two relations show that [Mg/Fe] increases with velocity dispersion. However, the slopes of the Mg_2-σ relation and the <Fe>-σ relation are best explained as due to changes in both abundances and ages as functions of the velocity dispersion (cf., Section 8.1).

The fact that there is no significant age term in the relations for [Mg/Fe] may indicate that [Mg/Fe] is set early in the evolutionary history of a galaxy and that later star formation episodes leading to a younger mean age of the stellar populations do not significantly alter [Mg/Fe].

8 THE SCALING RELATIONS REVISITED

The M/L ratio and the line indices are all correlated with the velocity dispersion. Only the M/L ratio is tighter correlated with the mass than with the velocity dispersion (e.g., JFK96, J97). The relations are shown on Fig. 11 for the Coma cluster sample. These scaling relations can all be understood as relations between the stellar populations and the velocity dispersions of the galaxies. In Table 4 we list the relations derived from the current sample as well as the relations from J97 (relations between the line indices and the velocity dispersions) and JFK96 (the relation between

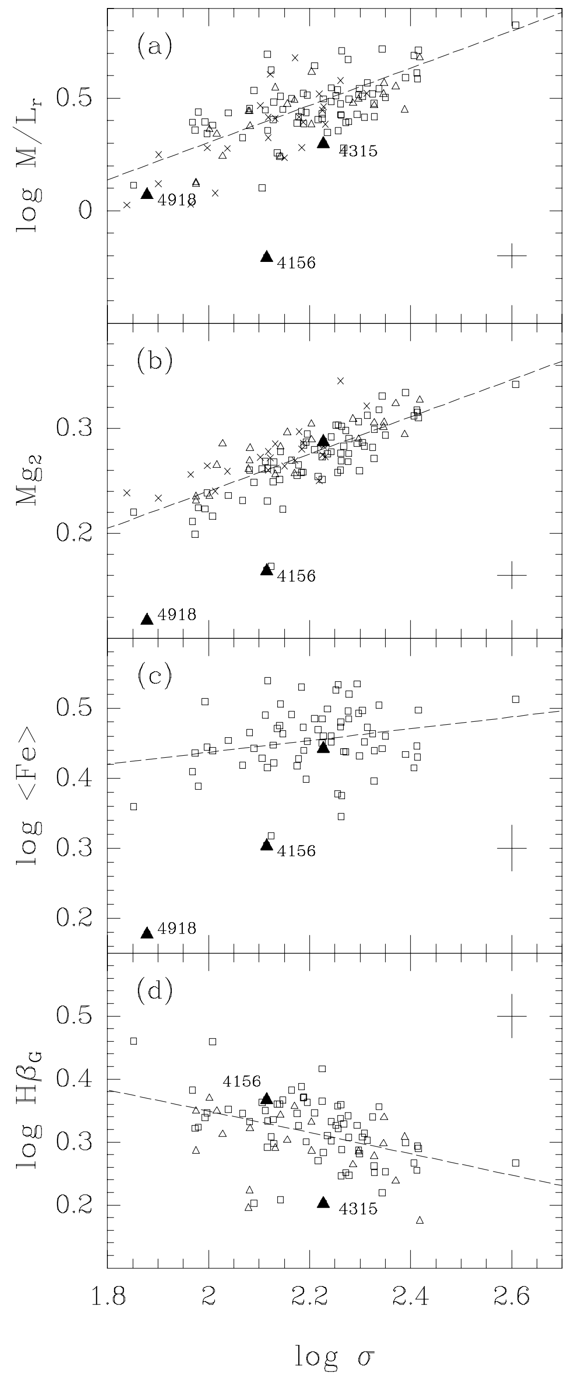

Figure 11. The M/L ratio and the line indices Mg_2, <Fe> and Hβ_G versus the velocity dispersion. The relations on the panels are the least squares fits given in Table 4 relation (2), (5), (8) and (11). Boxes – galaxies with <Fe> measured; triangles – galaxies with Hβ_G measured but no measurement of <Fe>; crosses – galaxies with no measurement of <Fe> and Hβ_G; filled triangles – galaxies with emission lines. Typical error bars are shown on the panels.

the M/L ratios and the velocity dispersions). The relations based on the Coma cluster sample were derived by minimizing either the sum of the absolute residuals in the direction of the y-axis or by a least squares fit with the residuals minimized in the direction of the y-axis. When minimizing the sum of the absolute residuals, the uncertainties on the coeffi-

Table 4. Scaling relations

Rel.	Ref.	Technique	N	Relation	rms[a]
1	J97	$\Sigma\vert\Delta p\vert$	250	$\mathrm{Mg}_2 = (0.196 \pm 0.009)\log\sigma - 0.155$	0.020
2	(1)	$\Sigma\Delta y^2$	112	$\mathrm{Mg}_2 = (0.177 \pm 0.014)\log\sigma - 0.114$	0.020
3	(1)	$\Sigma\vert\Delta y\vert$	112	$\mathrm{Mg}_2 = (0.175 \pm 0.012)\log\sigma - 0.108$	0.020
4	(1)	$\Sigma\Delta y^2$	68^b	$\mathrm{Mg}_2 = (0.212 \pm 0.017)\log\sigma - 0.198$	0.019
5	(1)	$\Sigma\vert\Delta y\vert$	68^b	$\mathrm{Mg}_2 = (0.203 \pm 0.016)\log\sigma - 0.177$	0.019
6	J97	$\Sigma\vert\Delta p\vert$	187	$\log \langle\mathrm{Fe}\rangle = (0.075 \pm 0.025)\log\sigma + 0.291$	0.045
7	(1)	$\Sigma\Delta y^2$	68	$\log \langle\mathrm{Fe}\rangle = (0.084 \pm 0.042)\log\sigma + 0.269$	0.045
8	(1)	$\Sigma\vert\Delta y\vert$	68	$\log \langle\mathrm{Fe}\rangle = (0.089 \pm 0.046)\log\sigma + 0.260$	0.045
9	(1)	$\Sigma\Delta y^2$	62^c	$\log \langle\mathrm{Fe}\rangle = (0.050 \pm 0.053)\log\sigma + 0.347$	0.045
10	(1)	$\Sigma\vert\Delta y\vert$	62^c	$\log \langle\mathrm{Fe}\rangle = (0.040 \pm 0.055)\log\sigma + 0.370$	0.045
11	J97	$\Sigma\vert\Delta p\vert$	101	$\log \mathrm{H}\beta_\mathrm{G} = (-0.231 \pm 0.082)\log\sigma + 0.825$	0.048
12	(1)	$\Sigma\Delta y^2$	90	$\log \mathrm{H}\beta_\mathrm{G} = (-0.169 \pm 0.038)\log\sigma + 0.687$	0.047
13	(1)	$\Sigma\vert\Delta y\vert$	90	$\log \mathrm{H}\beta_\mathrm{G} = (-0.146 \pm 0.044)\log\sigma + 0.642$	0.048
14	(1)	$\Sigma\Delta y^2$	68^b	$\log \mathrm{H}\beta_\mathrm{G} = (-0.197 \pm 0.042)\log\sigma + 0.756$	0.045
15	(1)	$\Sigma\vert\Delta y\vert$	68^b	$\log \mathrm{H}\beta_\mathrm{G} = (-0.160 \pm 0.050)\log\sigma + 0.676$	0.045
16	JFK96	$\Sigma\Delta y^2$	226	$\log M/L = (0.86 \pm 0.05)\log\sigma - 1.453$	0.11
17	(1)	$\Sigma\Delta y^2$	113	$\log M/L = (0.76 \pm 0.08)\log\sigma - 1.230$	0.11
18	(1)	$\Sigma\vert\Delta y\vert$	113	$\log M/L = (0.66 \pm 0.09)\log\sigma - 1.000$	0.11
19	(1)	$\Sigma\Delta y^2$	68^b	$\log M/L = (0.61 \pm 0.10)\log\sigma - 0.875$	0.11
20	(1)	$\Sigma\vert\Delta y\vert$	68^b	$\log M/L = (0.49 \pm 0.12)\log\sigma - 0.604$	0.11

Notes – References: J97 – Jørgensen (1997), JFK96 – Jørgensen et al. (1996), (1) – this paper. Techniques: $\Sigma|\Delta p|$ – the sum of the absolute residuals perpendicular to the relation has been minimized and the uncertainties derived with a boot-strap method. $\Sigma|\Delta y|$ – the sum of the absolute residuals has been minimized and the uncertainties derived with a boot-strap method. $\Sigma\Delta y^2$ – least squares fit. [a] rms scatter of the Coma cluster sample relative to the relation. [b] Only galaxies with available <Fe> are included; these galaxies have all parameters available. [c] Galaxies with $\log\sigma \le 2.0$ are excluded.

cients were derived by a boot-strap method. We minimize in the direction of the y-axis rather than perpendicular to the relations as done in J97 and JFK96, because we assume that the stellar populations are determined by the velocity dispersions of the galaxies. The differences between the relations derived using the three methods are fairly small, cf. Table 4. We have also derived the relations for the sub-sample of 68 galaxies for which all the spectroscopic parameters are available. None of the slopes derived for the sub-sample deviates from the slopes for the larger samples with more than 1.6 times the uncertainties of the differences. Therefore we do not expect the incompleteness of the sub-sample with all available parameters to significantly affect our results regarding the scaling relations.

Further, we have derived the scaling relations for the E and the S0 galaxies separately. We find no significant differences between the relations for the E and the S0 galaxies. This is in agreement with previous results by, e.g., JFK96 and J97.

In the following, we interpret the slopes of the scaling relations as due to changes in the mean ages and mean abundances as a function of the velocity dispersion. We then test (a) if this interpretation is consistent with the relations between the mean ages, the mean abundances and the velocity dispersions as derived in Sect. 7, and (b) if the observed rms scatter of the scaling relations is consistent with the rms scatter in the ages and abundances. The relation between the M/L ratios and the velocity dispersions is used for these tests rather than the FP or its interpretation as a relation between the M/L ratios and the masses. Using the M/L-σ relation makes the interpretation of scaling relations simpler, while the results still have implications for the FP.

From the approximate relations for the models given in Table 1 we derive by partial differentiation with respect to $\log\sigma$ the relations between the slopes of the scaling relations, ($\partial \mathrm{Mg}_2/\partial\log\sigma$, $\partial\log\langle\mathrm{Fe}\rangle/\partial\log\sigma$ and $\partial\log\mathrm{H}\beta_\mathrm{G}/\partial\log\sigma$) and the partial derivatives of the abundances and the ages,

$$\frac{\partial \mathrm{Mg}_2}{\partial\log\sigma} = 0.12\frac{\partial\log\mathrm{age}}{\partial\log\sigma} + 0.18\frac{\partial[\mathrm{Mg/H}]}{\partial\log\sigma} \tag{10}$$

$$\frac{\partial\log\langle\mathrm{Fe}\rangle}{\partial\log\sigma} = 0.13\frac{\partial\log\mathrm{age}}{\partial\log\sigma} + 0.26\frac{\partial[\mathrm{Fe/H}]}{\partial\log\sigma} \tag{11}$$

$$\frac{\partial\log\mathrm{H}\beta_\mathrm{G}}{\partial\log\sigma} = -0.27\frac{\partial\log\mathrm{age}}{\partial\log\sigma} - 0.13\frac{\partial[\mathrm{Fe/H}]}{\partial\log\sigma} \tag{12}$$

From Table 3 relation (2) and (5) we get by partial differentiation with respect to $\log\sigma$,

$$\frac{\partial[\mathrm{Mg/H}]}{\partial\log\sigma} = -0.80\frac{\partial\log\mathrm{age}}{\partial\log\sigma} + 1.21 \tag{13}$$

$$\frac{\partial[\mathrm{Fe/H}]}{\partial\log\sigma} = -0.62\frac{\partial\log\mathrm{age}}{\partial\log\sigma} + 0.06 \tag{14}$$

These two equations are consistent with the partial derivative of Table 3 relation (7).

Equations (10)-(14) form a set of five linear equations with the three unknown, $\partial[\mathrm{Mg/H}]/\partial\log\sigma$, $\partial[\mathrm{Fe/H}]/\partial\log\sigma$, and $\partial\log\mathrm{age}/\partial\log\sigma$. We use the least squares method to derive the values of the three unknown. For the slopes of the scaling relations derived by least squares fits to the current sample of Coma cluster sample (Table 4 relations [2], [7] and [12]), we find

$$\frac{\partial[\mathrm{Mg/H}]}{\partial\log\sigma} = 0.59 \pm 0.08 \tag{15}$$

$$\frac{\partial[\mathrm{Fe/H}]}{\partial\log\sigma} = -0.40 \pm 0.08 \tag{16}$$

$$\frac{\partial \log \mathrm{age}}{\partial \log \sigma} = 0.77 \pm 0.08 \tag{17}$$

Further, from the difference between equations (15) and (16) we get

$$\frac{\partial [\mathrm{Mg/Fe}]}{\partial \log \sigma} = 0.99 \pm 0.11 \tag{18}$$

The formal uncertainties are low. However, there are also uncertainties due to the adopted slopes of the scaling relations. If we use the relations derived for the Coma cluster sample by minimization of the sum of the absolute residuals we find 0.68, −0.33, and 0.65 for the three derivatives in Equations (15)-(17), respectively. This gives $\partial[\mathrm{Mg/Fe}]/\partial \log \sigma = 1.01$. If we use the relations derived for only the 68 galaxies with all available data (Table 4 relations [4], [7], and [14]), we find 0.50, −0.48, and 0.90, respectively. This gives $\partial[\mathrm{Mg/Fe}]/\partial \log \sigma = 0.98$.

The <Fe>-σ is very shallow and mostly driven by galaxies with velocity dispersions smaller than $100 \mathrm{km\,s^{-1}}$. If galaxies with velocity dispersions smaller than $100 \mathrm{km\,s^{-1}}$ are omitted the slope of the relation is not significantly different from zero (cf. Table 4 relations [9] and [10]; see also J97). If we assume that the slope of the <Fe>-σ relation is zero and use Table 4 relations (4) and (14) for the two other slopes, then we find 0.43, −0.55, and 0.97 for the three derivatives in equations (15)-(17), respectively. This gives $\partial[\mathrm{Mg/Fe}]/\partial \log \sigma = 0.98$.

Thus, the result for $\partial[\mathrm{Mg/Fe}]/\partial \log \sigma$ is very robust and does not depend significantly on the adopted slopes of the scaling relations. The rms scatter of the four determinations is only 0.01. The rms scatter of the determinations of $\partial[\mathrm{Mg/H}]/\partial \log \sigma$, $\partial[\mathrm{Fe/H}]/\partial \log \sigma$ and $\partial \log \mathrm{age}/\partial \log \sigma$ is 0.11, 0.10 and 0.14, respectively. We interpret the rms scatter as representative measures of the uncertainties due to the uncertainties in the slopes of the scaling relations.

As an experiment, we now assume that the [Mg/H] is a better metallicity indicator than [Fe/H], and that the slope of the $\mathrm{H}\beta_\mathrm{G}$-$\sigma$ relation depends on [Mg/H] rather than [Fe/H]. We substitute [Mg/H] for [Fe/H] in equation (12). Using the same technique as above and the slopes in Table 4 relations (4), (9), and (14), we then find 1.08, −0.02 and 0.16 for the three derivatives in equations (15)-(17), respectively, and $\partial[\mathrm{Mg/Fe}]/\partial \log \sigma = 1.10$. While this may appear as a solution that explains the slopes of the scaling relations as due mostly to variations in [Mg/H], we note that it contradicts the assumption that an abundance ratio [Mg/Fe] different from zero does not affect $\mathrm{H}\beta_\mathrm{G}$. This is assumption (c) in Section 4. Since we used this assumption in order to derive self-consistent ages and abundances for the galaxies, we do not consider this solution a self-consistent explanation of the slopes of the scaling relations.

We do not find any significant differences between the scaling relations or the age-metallicity-velocity dispersion relations followed by E and S0 galaxies, respectively. This is also reflected in the fact that if we derive the three derivatives in equation (15)-(17) using the relations derived for the E and the S0 galaxies separately, the results agree within the uncertainties. We find 0.56, −0.31, and 0.64 for the E galaxies, and 0.65, −0.20 and 0.67 for the S0 galaxies.

In the following we mainly use the results from equations (15)-(18), and briefly discuss the consequences of the other possible results.

8.1 The slopes of the scaling relations

Equations (15)-(17) represent the best solution to equations (10)-(14). However, that does not guarantee that the solution is in agreement with the empirically determined slopes of the scaling relations.

The slopes of the scaling relations predicted based on equations (15)-(17) are 0.199, −0.004, and −0.156 for the Mg_2-σ relation, the <Fe>-σ relation and the $\mathrm{H}\beta_\mathrm{G}$-$\sigma$ relation, respectively. These predicted slopes should be compared to the slopes given in Table 4 relations (2), (7) and (12). The largest deviation is for the <Fe>-σ relation, where the predicted slope deviates from the fitted slope with approximately twice the uncertainty of the fitted slope. However, for galaxies with velocity dispersions larger than $100\,\mathrm{km\,s^{-1}}$ it is likely that the slope of the <Fe>-σ relation is very close to zero (Table 4 relations [9] and [10], see also J97). For Mg_2-σ relation and the $\mathrm{H}\beta_\mathrm{G}$-$\sigma$ relation the predicted and the fitted slope agree within 1.5 times the uncertainty of the fitted slope.

It is not possible to explain the slopes in a consistent way by variations in the mean abundances only or by variations in the mean ages only. This can be seen as follows. Assume that the slopes are due to variations in the mean abundances only. The slope of the $\mathrm{H}\beta_\mathrm{G}$-$\sigma$ relation then implies that $\partial[\mathrm{Fe/H}]/\partial \log \sigma = 1.30$, while the slope of the <Fe>-σ relation implies that $\partial[\mathrm{Fe/H}]/\partial \log \sigma = 0.34$. Alternatively, the slope of the $\mathrm{H}\beta_\mathrm{G}$-$\sigma$ relation implies $\partial[\mathrm{Mg/H}]/\partial \log \sigma = 1.30$, while the slope of the Mg_2-σ relation implies that $\partial[\mathrm{Mg/H}]/\partial \log \sigma = 0.98$.

Next, assume that the slopes are due to variations in the mean ages only. From the slopes of the $\mathrm{H}\beta_\mathrm{G}$-$\sigma$ relation and the <Fe>-σ relation we get $\partial \log \mathrm{age}/\partial \log \sigma = 0.63$ and $\partial \log \mathrm{age}/\partial \log \sigma = 0.70$ respectively. However, the slope of the Mg_2-σ relation implies that $\partial \log \mathrm{age}/\partial \log \sigma = 1.45$.

We conclude that the solution given in equations (15)-(17) is consistent with the interpretation that the slopes of the scaling relations for the line indices are due to variations in both the mean ages and the mean abundances as functions of the velocity dispersions. See also Greggio (1997) for a discussion of the age and metallicity variations of stellar populations in E galaxies.

Next we test if the slope of the FP, here expressed as the slope of the relation between the M/L ratios and the velocity dispersions, is consistent with the variations in the mean ages and mean abundances as functions of the velocity dispersions as given in equations (15)-(17). Differentiation of the model prediction of the M/L ratio as a function of the mean age and mean metallicity (cf. Table 1) gives

$$\frac{\partial \log M/L}{\partial \log \sigma} = 0.67 \frac{\partial \log \mathrm{age}}{\partial \log \sigma} + 0.24 \frac{\partial [\mathrm{Fe/H}]}{\partial \log \sigma} \tag{19}$$

Using equations (15)-(17) we then find a predicted slope of

$$\frac{\partial \log M/L}{\partial \log \sigma} = 0.42 \tag{20}$$

while the fitted slope is 0.76 ± 0.08 (Table 4 relation [17]). The difference between the predicted slope and the fitted slope is 4.3 times the uncertainty of the fitted slope. If we use [Mg/H] instead of [Fe/H] in equation (19) and also make the (inconsistent) assumption that the slope of the $\mathrm{H}\beta_\mathrm{G}$-$\sigma$ relation depends on [Mg/H] rather than [Fe/H], then the predicted slope of the M/L-σ relation is 0.37.

The "steeper" slope of the FP may be due to one or more of the following effects, (a) variations in the fraction of dark matter as a function of the velocity dispersion (and the mass) as indicated by Fig. 6, (b) variations in the IMF as a function of the velocity dispersion, (c) changes in the luminosity profile shapes as a function of the velocity dispersion, and (d) non-homologous velocity dispersion profiles.

The required variation in the fraction of dark matter is $\partial \log(M_{\rm dark}/M_{\rm lum}+1)/\partial \log \sigma = 0.34$, consistent with Fig. 6(i). However, as noted in Sect. 3 we cannot with the present data disentangle variations in the fraction of dark matter from variations in the IMF and any non-homology of either the luminosity profiles or the velocity dispersion profiles.

Several recent studies have addressed the question of non-homology. Ciotti & Lanzoni (1996) modeled galaxies with luminosity profiles that follow the $R^{1/n}$-law rather than the $R^{1/4}$-law, and that have some degree of velocity anisotropy. They conclude that the velocity anisotropy cannot explain the slope of the FP, if the galaxies are structurally homologous. However, if they have $R^{1/n}$ profiles and n varies with luminosity, (e.g., Caon, Capaccioli, D'Onofrio 1993; Graham et al. 1996) then the combination of the velocity anisotropy and the variation of n may contribute to the slope of the FP. From simulations of dissipationless mergers, Capelato, de Carvalho & Carlberg (1995) also find that non-homologous velocity distribution and mass (luminosity) distribution can explain the slope of the FP. It is important to remember, that none of these studies of the role of non-homology have taken into account the disks present in both the S0 galaxies and in a large fraction of the E galaxies (cf. Jørgensen & Franx 1994).

8.2 The scatter of the scaling relations

Next we test if the scatter of the scaling relations is consistent with the scatter we find for the mean ages and abundances at a given velocity dispersion. The expected scatter in the scaling relations due to the scatter in the mean ages and abundances can be estimated from the expected relations between the line indices and the M/L ratio, and the ages and abundances (Table 1).

The derived mean ages and [Fe/H] are both uncorrelated with the velocity dispersion, see Figs. 6(f) and 8(f). As representative values for the rms scatter of the mean ages and of [Fe/H] we therefore use the scatter given in Table 2, 0.264 and 0.260 for log age and [Fe/H], respectively. The velocity dispersion and [Mg/H] are correlated, see Fig. 8(c). A least squares fit of [Mg/H] as a function of $\log \sigma$ gives [Mg/H]= $(0.98 \pm 0.18) \log \sigma - 1.93$, with an rms scatter of 0.227. We use this value as the rms scatter of [Mg/H] at a given velocity dispersion. The intrinsic rms scatter can be estimated as $\mathrm{rms_{int}} = (\mathrm{rms_{obs}}^2 - \sigma^2_{\rm meas})^{1/2}$ where $\sigma_{\rm meas}$ is the measurement error given in Table 2. The intrinsic rms scatter of the ages and [Fe/H] are 0.166 and 0.194, respectively (see Table 2). For [Mg/H], we find an intrinsic rms scatter of 0.175.

In order to take the correlation between the mean ages and the mean abundances into account, we determine the linear correlation coefficients between these. The linear correlation coefficient of the mean ages and [Fe/H] is −0.63. Because the [Mg/H] is correlated with the velocity dispersion, a direct determination of the linear correlation coefficient of the mean ages and [Mg/H] will lead to a correlation coefficient too small to correctly reflect the correlation between the mean ages and [Mg/H] at a given velocity dispersion. The sample was therefore divided in three velocity dispersion intervals and the linear correlation coefficient was derived for each sample. The mean of the determinations is −0.85, which we use as the linear correlation coefficient of the mean ages and [Mg/H].

Table 5. Scatter of the scaling relations

Relation	$\mathrm{rms_{obs}}$	$\mathrm{rms_{int}}$	$\mathrm{rms_{pred}}$	$\mathrm{rms_{pred,int}}$
$\mathrm{Mg_2}$-σ	0.020	0.018	0.022	0.018
<Fe>-σ	0.045	0.029	0.053	0.040
$\mathrm{H\beta_G}$-σ	0.047	0.027	0.056	0.035
M/L-σ	0.110	0.090	0.146	0.089

The expected rms scatter of the scaling relations was then derived as

$$\begin{aligned}\mathrm{rms_{pred}} = \big\{ & (a_i \, \mathrm{rms}(\log \mathrm{age}))^2 + (b_i \, \mathrm{rms}([\mathrm{M/H}]))^2 + \\ & 2 a_i b_i \, \mathrm{corr}(\log \mathrm{age}, [\mathrm{M/H}]) \, \mathrm{rms}(\log \mathrm{age}) \, \mathrm{rms}([\mathrm{M/H}]) \, \big\}^{1/2}\end{aligned} \quad (21)$$

where a_i and b_i are given in Table 1, corr(log age, [M/H]) is the linear correlation coefficient between log age and [M/H], and [M/H] refers to [Mg/H] or [Fe/H]. Table 5 lists the observed and the intrinsic rms scatter of the relations together with the predicted rms scatter derived using equation (21). Both the predicted rms scatter including the measurement uncertainties and the predicted intrinsic rms scatter were derived. The agreement between the scatter of the relations and the predicted scatter is very good. The only significant difference between the predictions and the actual (observed and intrinsic) scatter of the relations is for the intrinsic scatter of the <Fe>-σ. The predicted scatter is larger than the intrinsic scatter of the relation. If we use the scatter in [Mg/H], rather than the scatter in [Fe/H], to predict the scatter of the $\mathrm{H\beta_G}$-σ relation and the M/L-σ relation, we find $\mathrm{rms_{pred}}$=0.049 and 0.134 for the two relations, respectively. Thus, the predictions are slightly smaller than the values in Table 5, but also consistent with the observed scatter.

In summary, the rms scatter of the mean ages and abundances is consistent with, and can fully explain, the scatter of the scaling relations. Further, the correlation between the mean ages and the abundances keep the scatter of the relations lower than it would have been in the absence of such a correlation. The existence of a strong correlation between the mean ages and the abundances means that larger variations in the ages and abundances are possible while still maintaining the low scatter of the scaling relations. This was noted in a qualitative way by Worthey et al. (1995) and Worthey (1997). Our quantification of the effects adds support to Worthey's results. It is also possible that the correlation between the mean ages and the abundances is the main reason that the scatter of the FP does not depend significantly on the passband in which the photometry was obtained (cf. JFK96). The near-infrared FP may present a problem to this explanation of the low scatter. Pahre, Djorgovski & de Carvalho (1998) studied the FP for photometry obtained in the K-band and found the scatter of the FP to be equally low in this passband. The M/L ratios in the K-band have virtually no metal dependence if the models by Vazdekis et al. (1996) are used. For a high-mass IMF slope of $x = 1.35$ the models predict $\log M/L_K \approx 0.69 \log \mathrm{age} - 0.04[\mathrm{M/H}] - 0.81$. However, for the models by Worthey (1994) the metal dependence of the M/L ratios is close to zero for photometry in the I-band, not the K-band. It may require better models in the near-infrared to test whether the low scatter of the FP in the near-infrared is in agreement with rather large variations in the ages and the abundances and a strong correlation between the ages and the abundances.

9 CONCLUSIONS

The mean ages and abundances have been studied for a large sample of E and S0 galaxies in the Coma cluster. The photometry is from Jørgensen & Franx (1994), who presented photometry in Gunn r for the full sample. We present new spectroscopy for 71 galaxies in the cluster. Together with spectroscopic data from the literature, velocity dispersions and line indices are available for 115 galaxies. We have derived the mean ages and abundances ([Mg/H] and [Fe/H]) from the Mg_2 and <Fe> indices combined with either the $\mathrm{H}\beta_\mathrm{G}$ indices or the M/L ratio. We interpret the differences in the ages derived using the $\mathrm{H}\beta_\mathrm{G}$ indices and using the M/L ratios as a difference in the fraction of dark matter in the galaxies, or alternatively as a variation of the slope of the IMF.

We find that there are real variations in both the ages and the abundances. The intrinsic rms scatter of the ages is 0.17 dex, while the intrinsic rms scatter of [Mg/H], [Fe/H] and [Mg/Fe] is 0.2 dex. The ages of the galaxies are uncorrelated with the masses, luminosities and velocity dispersions (for ages based on $\mathrm{H}\beta_\mathrm{G}$).

The differences in the two age estimates are significant. Thus, there must be real variations in either the fraction of dark matter, the IMF slopes, or the degree of non-homology of the galaxies. Further, the most massive galaxies have the highest fraction of dark matter, and they have a smaller scatter in the ages and abundances than the lower mass galaxies.

The abundance ratio [Mg/Fe] increases with galaxy mass, luminosity and velocity dispersion. This is in agreement with previous results by Worthey et al. (1992) and J97. The result does not depend on whether the M/L ratio or the $\mathrm{H}\beta_\mathrm{G}$ index is used as the age sensitive parameter.

We establish the relations between the ages, the abundances and the velocity dispersion. The iron abundance [Fe/H] does not depend significantly on the velocity dispersion, while abundance ratio [Mg/Fe] does not depend significantly on the age. The magnesium abundance [Mg/H] depends on both the velocity dispersion and the age. These dependences may be indicate that [Mg/Fe] is set early in the evolutionary history of a galaxy and mostly determined by the velocity dispersion of the galaxy. Later episodes of star formation does not affect [Mg/Fe] significantly. Both [Fe/H] and [Mg/H] increases with later episodes of star formation, while [Mg/H] is also partly determined by the velocity dispersion of the galaxy.

The slopes of the Mg_2-σ, <Fe>-σ, and $\mathrm{H}\beta_\mathrm{G}$-$\sigma$ relations are consistent with how the age and the abundances vary as functions of the velocity dispersion. The slope of the Fundamental Plane (here expressed as the relation between the M/L ratio and the velocity dispersion) is steeper than predicted by these variations in ages and abundances. Changes in the fraction of dark matter as a function of the velocity dispersion (or mass) may contribute to the slope of the FP.

The relations between the ages, the abundances and the velocity dispersions allow substantial variations in the ages and abundances while still keeping the scatter of the scaling relations low. The rms scatter of the scaling relations is consistent with the rms scatter we find for the ages and the abundances, when the correlation between the ages and abundances is taken into account.

The established age-abundance-velocity dispersion relation and the derived variation of the ages and abundances as functions of the velocity dispersion may be used to predict the slopes and zero points of the scaling relations for intermediate redshift galaxies. Such predictions will depend on assumptions about the star formation history over the relevant look-back time. Predictions of this kind will be discussed in a future paper.

Acknowledgements: The staff at McDonald Observatory are thanked for assistance during the observations. B. Milvang-Jensen is thanked for providing part of the software used for this research. The anonymous referee is thanked for comments and suggestions that improved this paper. Support for this work was provided by NASA through grant number HF-01073.01.94A to IJ from the Space Telescope Science Institute, which is operated by the Association of Universities for Research in Astronomy, Inc., under NASA contract NAS5-26555. Part of this work was carried out while IJ was a Harlan J. Smith postdoctoral fellow at McDonald Observatory.

REFERENCES

Aaronson M., Cohen J. G., Mould J., Malkan M., 1978, ApJ, 223, 824
Bender R., Burstein D., Faber S. M., 1992, ApJ, 399, 462
Bertelli G., Bressan A., Chiosi C., Fagotto F., Nasi E., 1994, A&AS, 106, 275
Biviano A., Durret F., Gerbel D., le Fèvre O., Lobo C., Mazure A., Slezak E., 1995, A&A, 111, 265
Bressan A., Chiosi C., Tantalo R., 1996, A&A, 311, 425
Bruzual A. G., Charlot S., 1993, ApJ, 405, 538
Burstein D., Faber S. M., Gaskell C. M., Krumm N., 1984, ApJ, 287, 586
Burstein D., Davies R. L., Dressler A., Faber S. M., Lynden-Bell D., Terlevich R. J., Wegner G., 1988, in Kron R. G., Renzini A., eds., Towards Understanding Galaxies at Large Redshifts, Kluwer Academic Publishers, Dordrecht, p. 17
Buzzoni A., 1995, ApJS, 98, 69
Caldwell N., Rose J. A., Sharples R. M., Ellis R. S., Bower R. G., 1993, AJ, 106, 473
Caon N., Capaccioli M., D'Onofrio M., 1993, MNRAS, 265, 1013
Capelato H. V., de Carvalho R. R., Carlberg R. G., 1995, ApJ, 451, 525
Carollo C. M., Danziger I. J., Buson L., 1993, MNRAS, 265, 553
Ciotti L., Lanzoni B., 1997, A&A, 321, 724
Ciotti L., Lanzoni B., Renzini A., 1996, MNRAS, 282, 1
Davies R. L., Burstein D., Dressler A., Faber S. M., Lynden-Bell D., Terlevich R. J., Wegner G., 1987, ApJS, 64, 581

Davies R. L., Sadler E. M., Peletier R. F., 1993, MNRAS, 262, 650
Djorgovski S., Davis M., 1987, ApJ, 313, 59
Dressler A., 1980, ApJS, 42, 565
Dressler A., 1987, ApJ, 317, 1
Dressler A., Shectman S. A., 1988, AJ, 95, 284
Dressler A., Lynden-Bell D., Burstein D., Davies R. L., Faber S. M., Terlevich R. J., Wegner G., 1987, ApJ, 313, 42
Faber S. M., 1972, A&A, 20, 361
Faber S. M., Dressler A., Davies R. L., Burstein D., Lynden-Bell D., Terlevich R. J., Wegner G., 1987, in Faber S. M., ed., Nearly Normal Galaxies, New York, Springer-Verlag, p. 175
Faber S. M., Friel E. D., Burstein D., Gaskell C. M., 1985, ApJS, 57, 711
Faber S. M., Trager S. C., González J. J., Worthey G., 1995, in van der Kruit P. C., Gilmore G., eds., Stellar populations, IAU Symp. 164, Kluwer, Dordrecht, p. 249
Fisher D., Franx M., Illingworth G., 1995, ApJ, 448, 119
Fisher D., Franx M., Illingworth G., 1996, ApJ, 459, 110
Godwin J. G., Metcalfe N., & Peach J. V., 1983, MNRAS, 202, 113 (GMP)
González J. J., 1993, Ph.D. thesis, Univ. of California, Santa Cruz
González J. J., Gorgas J., 1995, in Buzzoni A., Renzini A., Serrano A., eds., Fresh Views on Elliptical Galaxies, ASP Conf. Ser. Vol. 86, Astron. Soc. Pac., San Francisco, p. 225
Gorgas J., Efstathiou G., Aragón-Salamanca A., 1990, MNRAS, 245, 217
Graham A., Lauer T. R., Colless M., Postman M., 1996, ApJ, 465, 534
Green E. M., Demarque P., King C. R., 1987, The Revised Yale Isochrones and Luminosity Functions, Yale University Observatory, New Haven
Greggio L., 1997, MNRAS, 185, 151
Guzmán R., Lucey J. R., Carter D., Terlevich R. J., 1992, MNRAS, 257, 187
Hjorth J., Madsen J., 1995, ApJ, 445, 55
Jørgensen I., 1997, MNRAS, 288, 161 (J97)
Jørgensen I., Hill G., 1998, submitted
Jørgensen I., Franx M., 1994, ApJ, 433, 553
Jørgensen I., Franx M., Kjærgaard P., 1995a, MNRAS, 273, 1097 (JFK95a)
Jørgensen I., Franx M., Kjærgaard P., 1995b, MNRAS, 276, 1341 (JFK95b)
Jørgensen I., Franx M., Kjærgaard P., 1996, MNRAS, 280, 167 (JFK96)
King I. R., 1966, AJ, 71, 64
Kuntschner H., Davies R. L., 1998, MNRAS, 295, L29
Lucey J. R., Guzmán R., Carter D., Terlevich, R. J., 1991, MNRAS, 253, 584
Mazure A., Proust D., Mathez G., Mellier Y., 1988, A&AS, 76, 339
O'Connell R. W., 1976, ApJ, 206, 370
Pahre M., Djorgovski S. G., de Carvalho R. R., 1998, AJ, 116, 1591
Peletier R. F., 1989, PhD Thesis, University of Groningen
Salpeter E. E., 1955, ApJ, 121, 161
Scalo J. M., 1986, Fund. Cosmic Phys., 11, 1
Trager S. C., Worthey G., Faber S. M., Burstein D., González J. J., 1998, ApJS, 116, 1
Tripicco M. J., Bell R. A., 1995, AJ, 110, 3035
VandenBerg D. A., 1985, ApJS, 58, 711
VandenBerg D. A., Bell R. A., 1985, ApJS, 58, 561
VandenBerg D. A., Laskarides P. G., 1987, ApJS, 64, 103
Vazdekis A., Casuso E., Peletier R. F., Beckman J. E., 1996, ApJS, 106, 307
Weiss A., Peletier R. F., Matteucci F., 1995, A&A, 296, 73
Worthey G., 1994, ApJS, 95, 107
Worthey G., 1996, in Leitherer C., Fritze-v. Alvensleben, Huchra J., eds., From Stars to Galaxies, ASP Conf. Ser. Vol. 98, p. 467
Worthey G., 1997, in Holt S., Mundy L. G., eds., Star Formation Near and Far, AIP Conf. Proc. Vol. 393, p. 525
Worthey G., Faber S. M., González J. J., 1992, ApJ, 398, 69
Worthey G., Faber S. M., González J. J., Burstein D., 1994, ApJS, 94, 687
Worthey G., Trager S. C., Faber S. M., 1995, in Buzzoni A., Renzini A., Serrano A., eds., Fresh Views on Elliptical Galaxies, ASP Conf. Ser. Vol. 86, Astron. Soc. Pac., San Francisco, p. 203

APPENDIX A: SPECTROSCOPY

Table A1 summarizes the instrumentation used for the spectroscopic observations. The parameters measured from the LCS and the FMOS spectra are given in Table A2 and Table A3, respectively. Table A4 gives the adopted mean values for the full sample of galaxies. The mean values for each galaxy are derived from the sources listed in Table A4, this includes the measurements from the LCS and the FMOS spectra as well as previously published data recalibrated by JFK95b.

Velocity dispersions are available for 116 E and S0 galaxies. The absorption line index Mg_2 is available for 115 of those galaxies, <Fe> have been measured for 71 galaxies, and 93 of the galaxies have available $\mathrm{H}\beta_\mathrm{G}$. The $\mathrm{H}\beta_\mathrm{G}$ index is related to the Lick/IDS $\mathrm{H}\beta$ index as $\mathrm{H}\beta_\mathrm{G} = 0.866\mathrm{H}\beta + 0.485$ (J97). All the spectroscopic parameters are centrally measured values corrected to a circular aperture with a diameter of 1.19 h^{-1} kpc (JFK95b; J97), $H_0 = 100\,\mathrm{h\,km\,s^{-1}\,Mpc^{-1}}$. Our technique for aperture correction are based on the mean radial gradients for E and S0 galaxies. As described in Section 2, we expect this to be inaccurate with no more than ± 0.0026 for the Mg_2. The effect on $\log$<Fe> and $\log \mathrm{H}\beta_\mathrm{G}$ are expected to be similarly small. The line indices are corrected for the effect of the velocity dispersion.

A1 The LCS data

Spectroscopic observations of 44 galaxies in the sample were obtained with the McDonald Observatory 2.7-m Telescope equipped with the Large Cassegrain Spectrograph (LCS). The observations were obtained March 14-21, 1994. During the same observing run 11 other galaxies were observed for comparison purposes. Velocity dispersions and Mg_2 indices for these galaxies have previously been published by Davies et al. (1987).

The spectra were reduced using standard methods. This includes correction for bias and dark current, and subtraction of scattered light. Correction for the pixel-to-pixel variation in the sensitivity was done with a normalized dome flat field derived as the mean of 70 individual flat fields. The pixel-to-pixel noise in the normalized flat field is $< 0.1\%$. The spectra were corrected for the slit function based on six high signal-to-noise sky flat fields. Due to flexure in the LCS, the slit function for each spectrum has to be shifted to match the current position of the slit relative to the CCD. The shifts were typically ± 4 pixels The uncertainty of the shifts are judge to be less than 0.25 pixel.

The spectra were cleaned for signal from cosmic-ray-events using the technique described in JFK95b. Wavelength

Table A1. Instrumentation for spectroscopy

	LCS spectra	FMOS spectra
Dates	March 14-21, 1994	April 21-26, 1995
Telescope	McD. 2.7-m	McD. 2.7-m
Instrument	LCS[a]	FMOS[b]
Grating/Grism	# 47, $1200\,\mathrm{l\,mm^{-1}}$	$300\,\mathrm{l\,mm^{-1}}$
Wavelength range	4879-5580Å	3810-7660Å
Resolution, σ[c]	0.97Å, $56\,\mathrm{km\,s^{-1}}$	4.25Å, $246\,\mathrm{km\,s^{-1}}$
Slit width	2 arcsec	...
Aperture[d]	$6\farcs35 \times 2''$, $4\farcs12$	$2\farcs6$
CCD	TI1, 800×800	Tek, 1024×1024
Read-out-noise	7.94 e^-	7.3 e^-
Gain	3.37 e^-/ADU	5.69 e^-/ADU
Spatial scale	$1\farcs27$	...
Galaxies in Coma	44	38
Other galaxies	11	...

Notes – [a] Large Cassegrain Spectrograph. [b] Fiber Multi-Object Spectrograph. [c] Derived as σ in fit with a Gaussian to lines in calibration spectra and to sky lines. The equivalent σ in $\mathrm{km\,s^{-1}}$ is given a 5175Å. [d] LCS spectra: The size of the rectangular aperture and the equivalent diameter of a circular aperture is given, cf. JFK95b. FMOS spectra: the diameter of the fibers is given.

calibrations were established from argon lamp spectra taken interdispersed with the observations. The rms scatter of the wavelength calibration is typically 0.06Å. The spectra were rectified using the corresponding wavelength calibration and the spectra themselves (to correct for the distortion in the spatial direction). We checked the stability of the wavelength calibration from exposure to exposure from the position of the 5577Å skyline. This gives an rms scatter of the wavelength calibration of 0.12Å, equivalent to $7\,\mathrm{km\,s^{-1}}$. The resolution is very stable, showing a rms scatter of only 0.036Å, equivalent to $2\,\mathrm{km\,s^{-1}}$ at 5175Å.

Observations of spectrophotometric standard stars (Hiltner 600, GD 190) were used to calibrate the spectra to a relative flux scale before the line indices were derived. The central velocity dispersion and the line indices Hβ, H$\beta_{\rm G}$, Mg_1, Mg_2, Mgb and <Fe> were derived using the methods described in JFK95b and J97. The velocity dispersions and the indices were corrected for to a standard aperture size with diameter $1.19\,h^{-1}\,\mathrm{kpc}$, and the indices were corrected for the effect of the velocity disperson. The techniques described in JFK95b and J97 were used. The aperture size used for the observations is given in Table A1.

Fig. A1 and Table A5 summarize the comparison between the parameters derived from the LCS spectra and literature data. We add 0.020 to our measurements of the Mg_2 indices in order to bring them onto the Lick/IDS system. The offset is due to the difference in calibration of these spectra and the procedure used for the Lick/IDS spectra (Trager et al. 1998).

A2 The FMOS data

Observations of 38 galaxies in the sample were obtained with the McDonald Observatory 2.7-m Telescope equipped with the Fiber Multi-Object Spectrograph (FMOS) April 21-26, 1995. FMOS is a grism spectrograph with 90-100 fibers and a field of view of 66 arcmin diameter. The spectra were obtained as part of a program to measure redshifts of fainter galaxies in the Coma cluster. The reductions and determination of the redshifts are described in detail in Jørgensen & Hill (1998). Here we will concentrate on the determination and calibration of the line indices for the galaxies included in the present sample.

The FMOS spectra have a spectral resolution of $\approx$ 10Å FWHM. This is sufficient to derive line indices, while we cannot derive velocity dispersions from these spectra. The resolution varies slightly with fiber position on the spectrograph entrance slit, and with the wavelength. The spectra were calibrated to a relative flux scale based on observations of spectrophotometric standard stars (HD192281, Wolf 1346) through a few of the fibers. Then the line indices were derived.

We established the calibrations to the Lick/IDS system as follows. All the available LCS spectra described in Sect. A.1.1 were convolved to the various resolutions found for the FMOS spectra. The variation of the resolution as a function of the wavelength was taken into account. Then we derived the line indices from the convolved spectra and established the transformations between the indices derived from the LCS spectra and the line indices derived from the convolved LCS spectra. The transformations were assumed to have the form

$$\mathrm{index(LCS)} = \alpha\, \mathrm{index(conv\,LCS)} + \beta \qquad \text{(A1)}$$

Transformation were established for each fiber position. For all indices, the coefficient α was typically between 1.0 and 1.2. β depends on the index, we find typically $\beta(\mathrm{H}\beta) = -0.13$, $\beta(\mathrm{H}\beta_{\rm G}) = -0.004$, $\beta(\mathrm{Mg}_1) = 0.001$, $\beta(\mathrm{Mg}_2) = 0.000$, $\beta(\mathrm{Mgb}) = 0.13$, $\beta(\mathrm{Fe5270}) = -0.005$ and $\beta(\mathrm{Fe5335}) = 0.024$. The transformations were applied and the line indices were aperture corrected and corrected for the velocity dispersion. The techniques described in J97 were used. After this calibration small offsets between the measured line indices and the Lick/IDS system are still present. These offsets are most likely due to failure to accurately match the resolutions of the spectra and to uncertainties in the spectrophotometric calibration. The uncertainty in the spectrophotometric calibration affects mostly the indices Mg_1 and Mg_2. The offsets were derived by comparison of the LCS calibrated data with the FMOS data for the galaxies in common. The following offsets were added to the FMOS data. $\Delta\mathrm{H}\beta$=0.31, $\Delta\mathrm{H}\beta_{\rm G}$ = 0.16, $\Delta\mathrm{Mg}_1$=0.023, $\Delta\mathrm{Mg}_2$=0.029, ΔMgb=0.020, and Δ<Fe>=0.22. Fig. A2 shows the comparison of the FMOS data with the LCS data and with Mg_2 from the literature (as calibrated by JFK95b). The FMOS data in this figure are calibrated to the Lick/IDS system as described above.

A3 The literature data

We use the velocity dispersions and Mg_2 indices as given by JFK95b. These data are from from Davies et al. (1987), Dressler (1987), Lucey et al. (1991) and Guzmán et al. (1992) and were calibrated to a consistent system by JFK95b.

We have transformed the Hδ strengths determined by Caldwell et al. (1993) to H$\beta_{\rm G}$. We have 42 galaxies in common with Caldwell et al. However, a direct transformation between Hδ and H$\beta_{\rm G}$ based on these galaxies turns out to be rather uncertain. Instead we derive the transformation

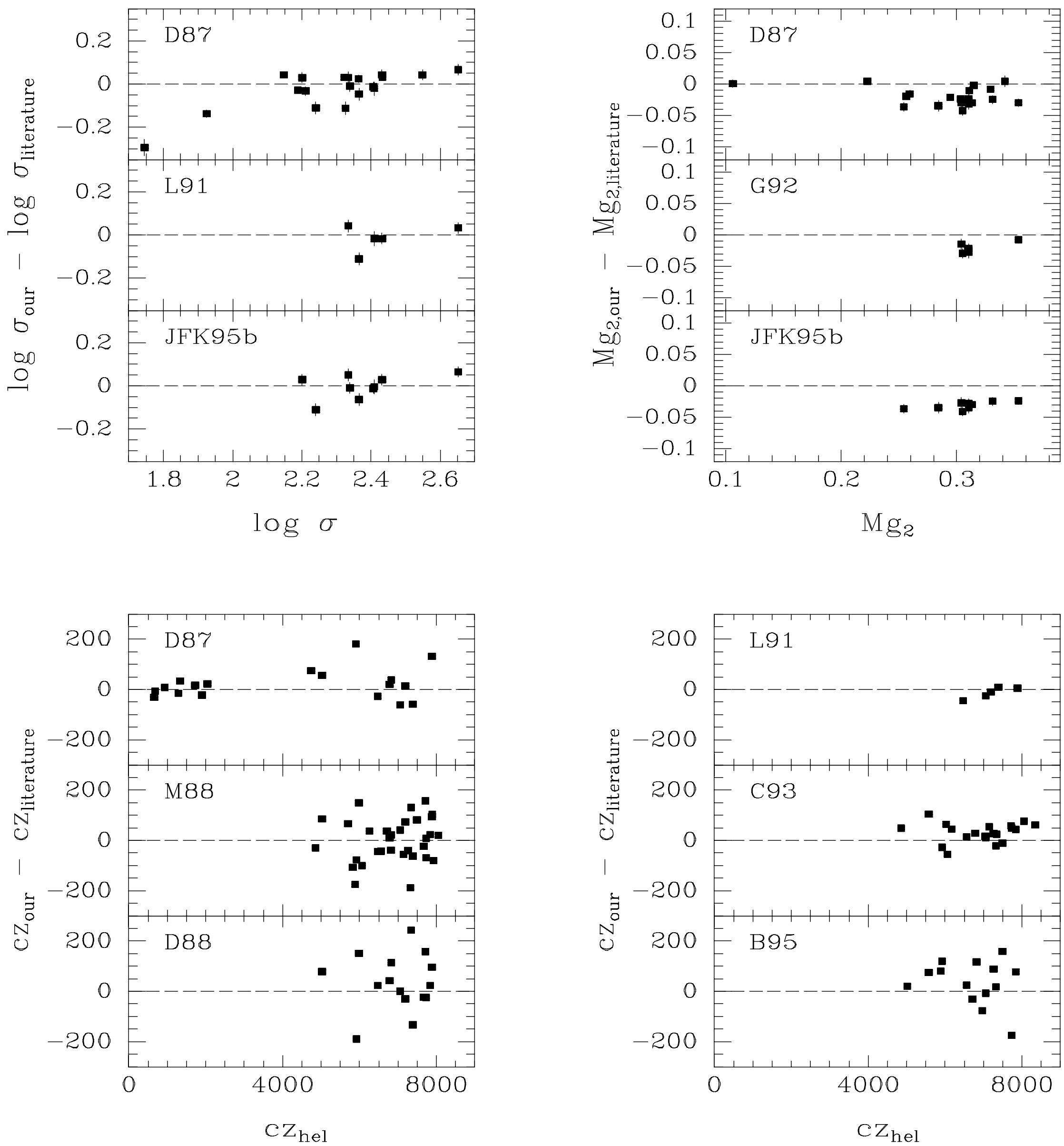

Figure A1. Comparison between the spectroscopic parameters derived from the LCS spectra and literature data. Our Mg_2 measurements shown on this figure have not yet been offset to consistency with the Lick/IDS system. The velocity dispersions and Mg_2 from Lucey et al. (1991) and Guzmán et al. (1992), respectively, have not been offset to consistency with Davies et al. (1987), see Table A5 and JFK95b. References: D87 – Davies et al. (1987); L91 – Lucey et al. (1991); G92 – Guzmán et al. (1992); JFK95b – Jørgensen et al. (1995b); M88 – Mazure et al. (1988); D88 – Dressler & Shectman (1988); C93 – Caldwell et al. (1993); B95 – Biviano et al. (1995). The data from JFK95b are literature data recalibrated to a consistent system.

by requiring that the relation between $H\beta_G$ and the velocity dispersion should be equivalent to the relation between $H\delta$ and the velocity dispersion. Fig. A3 shows the two relations. The resulting transformation is

$$\log H\beta_G = 0.50 \log H\delta + 0.16 \quad \text{(A2)}$$

with an rms scatter of 0.06 in $\log H\beta_G$. This uncertainty is equivalent to an uncertainty of the derived ages of about 0.016 dex. Since both $H\beta_G$ and $H\delta$ are line indices defined from on-line and off-line passbands, it cannot be expected that the transformation in equation (A2) reflects the expected difference in the strength of the two Balmer lines. We use $H\beta_G$ derived from $H\delta$ only for those 22 galaxies with no direct measurement of $H\beta_G$.

Table A5. External comparison of spectroscopic parameters from LCS spectra

Source	N	$<\Delta cz_{\rm hel}>$	rms of $\Delta cz_{\rm hel}$	$<\Delta \log \sigma>$	rms of $\Delta \log \sigma$	$<\Delta {\rm Mg}_2>$	rms of $\Delta {\rm Mg}_2$
Davies et al. (1987)[a]	19	21[b]	61	−0.002[c]	0.052[c]	−0.020	0.013
Lucey et al. (1991)	5	−13	23	−0.014	0.060		
Guzmán et al. (1992)	5					−0.020	0.010
Jørgensen et al. (1995b)[d]	9			−0.003	0.056	−0.031	0.006
Mazure et al. (1988)	32	0	87				
Dressler & Shectman (1988)	15	35	112				
Caldwell et al. (1993)	20	31	39				
Biviano et al. (1995)	14	35	88				

Notes – Differences calculated as "LCS"–"literature". The data from Lucey et al. and Guzmán et al. are from the same observations. The data have not been offset to consistency with Davies et al. The offsets are $\log \sigma$(Davies et al.)=$\log \sigma$(Lucey et al.)–0.020; $\rm Mg_2$(Davies et al.)=$\rm Mg_2$(Guzmán et al.)+0.010 (cf. JFK95b). [a] mean of individual determinations, velocity dispersions and $\rm Mg_2$ indices are corrected following JFK95b. [b] NGC 4841B = GMP4806 omitted. Our $cz_{\rm hel}$ is $532\,{\rm km\,s^{-1}}$ larger than the determination from Davies et al., while it is in agreement with the value from Mazure et al. (1988). [c] Two galaxies with $\log \sigma < 2.0$ omitted. [d] Data from other sources calibrated to a homogeneous system.

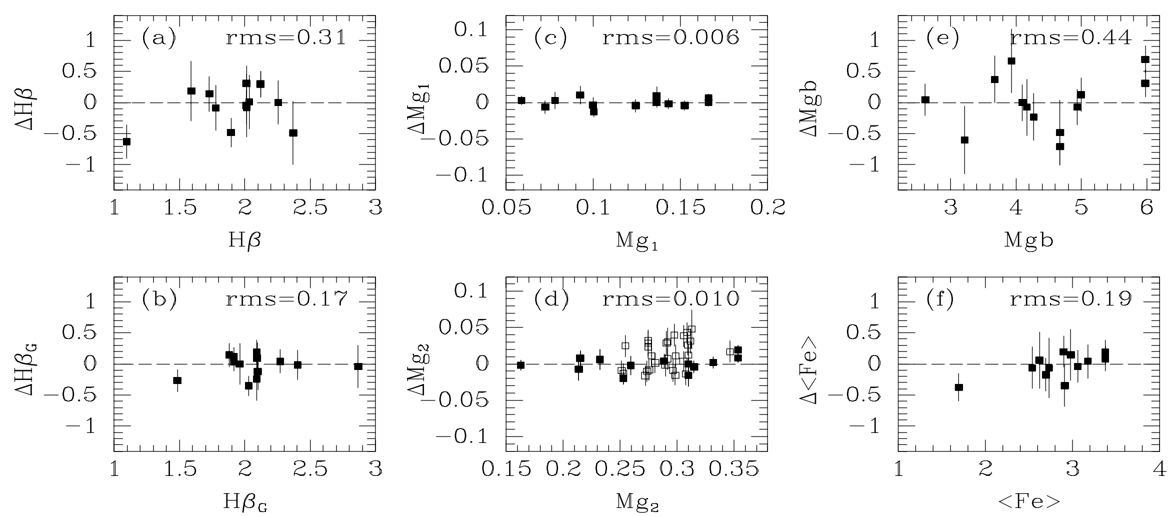

Figure A2. Comparison of line indices derived from the FMOS spectra with line indices from the LCS spectra and from the literature. Filled symbols – comparison with indices from LCS spectra; open symbols – comparison with literature data (JFK95b), only $\rm Mg_2$. The indices from the FMOS spectra have been calibrated to the Lick/IDS system, see text. The rms scatter of the comparisons with the LCS data are given in the panels. The rms scatter of the $\rm Mg_2$ comparison when all the available data are included is 0.019.

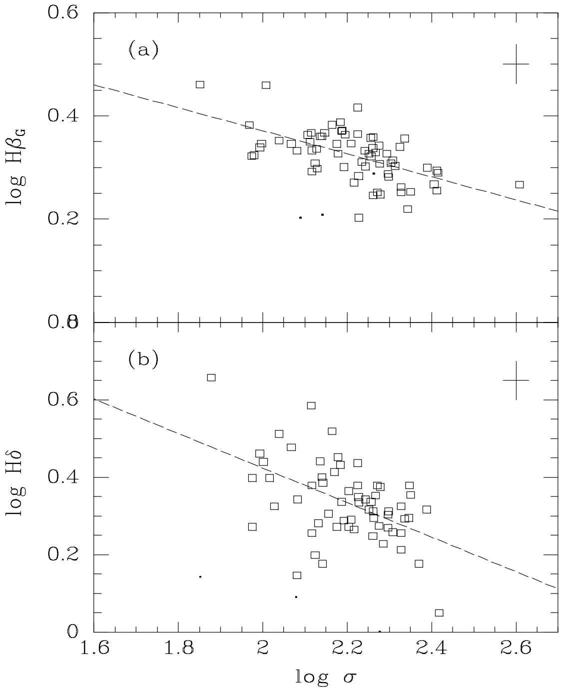

Figure A3. Relations between the Balmer line indices and the velocity dispersion. The $H\beta_G$ measurements and the velocity dispersions are the adopted mean values (Table A4). The $H\delta$ measurements are from Caldwell et al. (1993). Large boxes – measurements with uncertainties on $\log H\beta_G$ and $\log H\delta$ are smaller than 0.065 and 0.10, respectively. Measurements with larger uncertainty are shown as points. These galaxies were omitted from the determination of the relations. The relations are (a) $\log H\beta_G = -0.223 \log\sigma + 0.817$ and (b) $\log H\delta = -0.446 \log\sigma + 1.315$. The relations are used to derive the transformation between $H\beta_G$ and $H\delta$.

TABLE A2

Spectroscopic parameters, LCS spectra

Galaxy	$cz_{\rm hel}$	$\log \sigma$	Hβ	H$\beta_{\rm G}$	Mg$_1$	Mg$_2$	Mgb	<Fe>	S/N
1750	7882	2.409	1.59	1.97	0.122	0.311	5.61	2.69	24.2
		0.032	0.29	0.19	0.007	0.009	0.29	0.27	
1853	5821	2.294	1.79	2.12	0.124	0.286	3.93	3.42	32.3
		0.021	0.21	0.15	0.005	0.007	0.23	0.20	
2157	7341	2.277	1.88	2.03	0.116	0.276	4.30	3.05	36.5
		0.019	0.19	0.13	0.005	0.006	0.20	0.18	
2237	6708	1.997	2.25	2.22	0.072	0.238	3.97	2.78	28.3
		0.026	0.24	0.16	0.006	0.007	0.26	0.23	
2259	6941	2.008	2.37	2.87	0.092	0.214	3.21	2.73	22.2
		0.033	0.31	0.21	0.008	0.009	0.33	0.29	
2390	5020	2.339	1.09	1.48	0.152	0.331	4.99	2.89	32.8
		0.026	0.21	0.15	0.005	0.007	0.22	0.20	
2393	8341	2.124	1.82	2.03	0.048	0.169	3.17	2.08	24.5
		0.035	0.28	0.19	0.007	0.008	0.30	0.27	
2413	7672	2.235	1.82	2.04	0.113	0.276	4.30	3.15	30.5
		0.023	0.23	0.15	0.006	0.007	0.24	0.21	
2495	7928	2.106	2.13	2.31	0.101	0.261	4.19	2.68	29.3
		0.025	0.23	0.16	0.006	0.007	0.25	0.22	
2629	5986	2.188	2.30	2.35	0.118	0.284	4.53	2.75	29.3
		0.026	0.23	0.16	0.006	0.007	0.25	0.22	
2651	7728	1.993	1.85	2.18	0.084	0.223	3.58	3.23	28.3
		0.028	0.24	0.16	0.006	0.007	0.26	0.23	
2776	5907	2.112	2.01	2.27	0.100	0.253	4.10	3.06	28.3
		0.024	0.24	0.16	0.006	0.007	0.26	0.23	
2912	6785	2.201	2.20	2.35	0.090	0.254	4.12	2.97	29.0
		0.024	0.24	0.16	0.006	0.007	0.25	0.22	
2921	6470	2.652	2.12	1.91	0.166	0.354	5.98	3.37	38.2
		0.025	0.18	0.12	0.005	0.006	0.19	0.17	
2956	6562	2.117	1.82	2.15	0.112	0.262	4.29	3.46	24.2
		0.027	0.29	0.19	0.007	0.009	0.30	0.27	
3068	7728	1.979	1.71	2.11	0.077	0.224	3.71	2.45	25.6
		0.030	0.27	0.18	0.007	0.008	0.29	0.26	
3328	7622	2.147	2.08	2.33	0.047	0.223	4.22	2.91	32.5
		0.025	0.21	0.14	0.005	0.006	0.22	0.20	
3329	7191	2.432	2.01	2.09	0.136	0.305	4.67	3.17	28.0
		0.025	0.25	0.17	0.006	0.008	0.26	0.23	
3656	7834	2.116	1.59	1.96	0.078	0.232	3.93	2.62	28.0
		0.031	0.25	0.17	0.006	0.007	0.26	0.23	
3661	5699	2.255	2.03	2.28	0.108	0.258	3.92	2.39	28.3
		0.025	0.24	0.16	0.006	0.007	0.26	0.23	
3730	7059	2.334	1.57	1.94	0.143	0.304	4.50	3.11	25.6
		0.028	0.27	0.18	0.007	0.008	0.28	0.25	
3818	8048	2.298	1.63	1.91	0.109	0.259	4.21	2.70	26.3
		0.025	0.26	0.18	0.006	0.008	0.28	0.25	
3879	6031	2.136	2.10	2.29	0.117	0.260	4.11	2.96	27.4
		0.026	0.25	0.17	0.006	0.008	0.27	0.24	
3997	5923	2.327	1.57	1.83	0.124	0.271	4.18	2.49	27.7
		0.027	0.25	0.17	0.006	0.008	0.26	0.24	
4130	6821	2.262	1.97	2.29	0.124	0.276	4.71	3.02	29.6
		0.023	0.23	0.16	0.006	0.007	0.24	0.22	
4156	7718	2.115	1.89	2.03	0.059	0.163	2.61	1.69	32.3
		0.035	0.21	0.15	0.005	0.006	0.23	0.21	
4206	7051	2.068	1.91	2.22	0.084	0.231	4.26	2.62	29.9
		0.024	0.23	0.16	0.006	0.007	0.24	0.22	
4308	6707	1.973	1.92	2.10	0.048	0.199	3.69	2.73	22.6
		0.034	0.30	0.21	0.007	0.009	0.32	0.29	
4313	7895	2.128	1.80	2.17	0.095	0.249	4.29	2.80	28.0
		0.026	0.25	0.17	0.006	0.007	0.26	0.23	
4379	7495	2.267	1.74	2.13	0.114	0.283	4.24	2.74	48.7
		0.016	0.14	0.10	0.004	0.004	0.15	0.13	
4391	7202	1.968	2.25	2.40	0.072	0.215	3.67	2.54	28.7
		0.027	0.24	0.16	0.006	0.007	0.26	0.23	
4499	7149	2.217	1.82	1.86	0.096	0.254	4.49	2.94	28.0
		0.026	0.25	0.17	0.006	0.007	0.26	0.23	
4626	6969	2.090	1.38	1.59	0.089	0.249	4.83	2.77	15.4
		0.044	0.45	0.31	0.011	0.014	0.46	0.42	
4653	5885	2.195	1.93	2.31	0.120	0.295	4.83	2.83	32.5
		0.021	0.21	0.14	0.005	0.007	0.22	0.20	
4664	6063	2.140	2.27	2.29	0.091	0.251	3.91	2.99	29.0
		0.025	0.24	0.16	0.006	0.007	0.25	0.22	
4679	6168	1.852	2.64	2.89	0.077	0.220	3.28	2.29	25.3
		0.032	0.27	0.18	0.007	0.008	0.29	0.26	
4792	7261	2.175	1.98	2.22	0.092	0.255	4.72	2.62	23.4
		0.034	0.29	0.20	0.007	0.009	0.31	0.28	
4794	7322	2.272	1.60	1.78	0.116	0.298	4.77	2.74	27.0
		0.029	0.26	0.18	0.006	0.008	0.27	0.24	

TABLE A2—*Continued*

Galaxy	$cz_{\rm hel}$	$\log\sigma$	Hβ	H$\beta_{\rm G}$	Mg$_1$	Mg$_2$	Mgb	<Fe>	S/N
4806	6261	2.240	1.78	2.09	0.124	0.284	4.27	2.91	23.8
		0.029	0.29	0.20	0.007	0.009	0.30	0.27	
4822	6822	2.406	1.73	1.88	0.143	0.313	4.93	2.69	33.4
		0.022	0.21	0.14	0.005	0.006	0.22	0.20	
4866	8211	2.081	2.03	2.10	0.100	0.259	4.16	2.98	24.9
		0.029	0.28	0.19	0.007	0.008	0.29	0.26	
4907	5579	2.262	1.43	1.76	0.105	0.269	4.44	2.21	28.3
		0.030	0.25	0.17	0.006	0.007	0.25	0.23	
4918	4859	1.878	-6.28	-5.38	0.037	0.117	3.12	1.50	24.2
		0.048	0.35	0.24	0.007	0.008	0.31	0.28	
4928	7387	2.365	1.36	1.85	0.139	0.310	4.74	2.60	29.3
		0.028	0.24	0.16	0.006	0.007	0.25	0.22	
N2320	5906	2.548	0.73	1.10	0.147	0.311	5.21	2.68	37.0
		0.024	0.19	0.13	0.005	0.006	0.20	0.18	
N2513	4736	2.433	1.66	1.81	0.153	0.329	5.17	2.98	44.8
		0.017	0.16	0.11	0.004	0.005	0.16	0.15	
N2778	2038	2.189	···	···	0.139	0.303	4.58	2.84	57.3
		0.014	···	···	0.003	0.004	0.12	0.11	
N2974	1902	2.365	···	···	0.142	0.294	4.49	2.87	42.7
		0.018	···	···	0.004	0.005	0.17	0.15	
N3156	1330	1.746	···	···	0.014	0.106	1.63	1.91	33.9
		0.038	···	···	0.005	0.006	0.23	0.19	
N3377	683	2.150	···	···	0.109	0.256	3.83	2.68	54.1
		0.015	···	···	0.003	0.004	0.13	0.12	
N3379	930	2.325	···	···	0.146	0.315	4.66	2.66	61.9
		0.014	···	···	0.003	0.003	0.12	0.11	
N3605	654	1.926	···	···	0.084	0.222	3.35	2.88	42.3
		0.018	···	···	0.004	0.005	0.17	0.15	
N3640	1287	2.212	···	···	0.108	0.259	3.86	2.90	33.9
		0.021	···	···	0.005	0.006	0.21	0.19	
N4526	633	2.346	···	···	0.121	0.279	4.36	2.90	84.4
		0.011	···	···	0.002	0.003	0.09	0.08	
N5846	1726	2.327	···	···	0.166	0.342	4.75	2.63	25.6
		0.029	···	···	0.007	0.008	0.28	0.26	

NOTE.— Galaxy identifications from Godwin et al. (1983), except for the last 11 galaxies in the table for which NGC numbers are given. The radial velocity, $cz_{\rm hel}$, is given in km s^{-1} and corrected to the heliocentric system. <Fe>=(Fe5270+Fe5335)/2. The S/N ratio is given per Ångström. Internal uncertainties of the velocity dispersions and the line indices are given in the second line for each galaxy. The velocity dispersions and the line indices have been aperture corrected to $2r_{\rm norm} = 1.19{\rm h}^{-1}$kpc, equivalent to $3\farcs4$ at the distance of the Coma cluster. The line indices are consistent with the Lick/IDS system and corrected to zero velocity dispersion.

TABLE A3
SPECTROSCOPIC PARAMETERS, FMOS SPECTRA

Galaxy	Hβ	Hβ_G	Mg$_1$	Mg$_2$	Mgb	<Fe>	S/N
2259	2.86	2.91	0.082	0.221	3.82	2.79	17.0
	0.40	0.27	0.010	0.012	0.43	0.38	
2347	2.36	2.44	0.102	0.246	3.87	3.39	19.2
	0.36	0.24	0.009	0.011	0.38	0.34	
2390	1.72	1.75	0.157	0.330	4.87	2.70	44.4
	0.16	0.11	0.004	0.005	0.16	0.15	
2417	2.36	2.19	0.101	0.284	4.48	2.90	32.9
	0.21	0.14	0.005	0.006	0.22	0.20	
2440	1.67	1.78	0.120	0.298	4.81	2.75	47.3
	0.15	0.10	0.004	0.004	0.15	0.14	
2535	1.72	1.62	0.103	0.261	4.15	3.20	15.0
	0.47	0.32	0.011	0.014	0.49	0.43	
2541	1.87	1.92	0.115	0.283	4.74	2.89	63.9
	0.11	0.07	0.003	0.003	0.11	0.10	
2551	2.24	2.25	0.083	0.230	3.33	2.84	29.1
	0.24	0.16	0.006	0.007	0.25	0.22	
2727	2.48	2.41	0.095	0.258	4.34	3.10	25.2
	0.27	0.19	0.007	0.008	0.29	0.26	
2776	2.09	2.23	0.113	0.273	4.10	3.10	53.1
	0.13	0.09	0.003	0.004	0.14	0.12	
2798	1.67	2.06	0.114	0.284	4.27	2.83	37.4
	0.19	0.13	0.005	0.006	0.19	0.18	
2921	1.82	1.84	0.163	0.340	5.47	3.23	96.2
	0.07	0.05	0.002	0.002	0.08	0.07	
2922	1.73	2.09	0.133	0.306	5.16	3.42	26.5
	0.26	0.18	0.006	0.008	0.27	0.25	
2975	2.09	2.12	0.107	0.266	4.16	2.68	84.1
	0.08	0.06	0.002	0.002	0.09	0.08	
3055	1.78	2.01	0.133	0.314	4.69	2.97	42.8
	0.16	0.11	0.004	0.005	0.17	0.15	
3073	2.03	2.12	0.121	0.302	4.61	3.36	48.0
	0.14	0.10	0.004	0.004	0.15	0.14	
3165	2.28	2.32	0.095	0.249	3.94	2.82	53.1
	0.12	0.08	0.003	0.003	0.12	0.11	
3170	2.12	2.22	0.113	0.279	4.44	3.06	47.2
	0.15	0.10	0.004	0.004	0.15	0.14	
3201	2.15	2.18	0.098	0.261	3.92	2.97	58.2
	0.12	0.08	0.003	0.004	0.13	0.11	
3296	1.61	1.77	0.131	0.288	4.60	3.31	29.9
	0.23	0.16	0.006	0.007	0.24	0.22	
3329	1.71	1.90	0.136	0.310	5.38	3.13	48.9
	0.14	0.10	0.004	0.004	0.15	0.13	
3367	1.85	2.00	0.120	0.285	4.79	2.50	29.3
	0.24	0.16	0.006	0.007	0.24	0.22	
3390	2.75	2.61	0.104	0.262	4.02	3.05	20.7
	0.33	0.22	0.008	0.010	0.35	0.31	
3400	2.14	2.27	0.156	0.322	4.66	3.19	25.2
	0.27	0.19	0.007	0.008	0.29	0.26	
3414	1.85	2.00	0.128	0.292	4.70	2.88	32.3
	0.22	0.15	0.005	0.006	0.22	0.20	
3639	1.77	1.79	0.145	0.280	4.87	2.89	18.9
	0.37	0.25	0.009	0.011	0.38	0.35	
3656	1.40	1.96	0.075	0.226	3.26	2.56	17.0
	0.41	0.28	0.010	0.012	0.44	0.39	
3660	2.13	1.98	0.107	0.266	4.11	2.64	46.5
	0.15	0.10	0.004	0.004	0.16	0.14	
3761	2.10	2.20	0.102	0.265	4.40	3.13	59.4
	0.12	0.08	0.003	0.003	0.12	0.11	
3792	1.82	1.99	0.147	0.330	5.36	2.71	29.8
	0.23	0.16	0.006	0.007	0.24	0.22	
4017	2.24	1.94	0.116	0.265	3.79	2.37	8.9
	0.77	0.53	0.019	0.023	0.83	0.75	
4156	2.38	2.38	0.056	0.165	2.57	2.07	76.8
	0.09	0.06	0.002	0.003	0.10	0.09	
4230	2.10	2.15	0.133	0.268	4.34	2.83	27.5
	0.25	0.17	0.006	0.008	0.26	0.24	
4315	1.35	1.59	0.130	0.288	4.37	2.77	52.5
	0.13	0.09	0.003	0.004	0.14	0.12	
4391	2.25	2.42	0.079	0.207	3.30	2.60	26.8
	0.26	0.17	0.006	0.008	0.28	0.24	
4806	1.87	2.00	0.128	0.285	4.50	3.26	33.1
	0.21	0.14	0.005	0.006	0.22	0.20	
4822	1.59	1.74	0.145	0.319	5.01	2.87	38.1
	0.18	0.13	0.005	0.006	0.19	0.17	
4866	2.02	2.22	0.103	0.261	4.24	2.83	20.9
	0.33	0.22	0.008	0.010	0.35	0.31	

NOTE.— Galaxy identifications from Godwin et al. (1983). <Fe>=(Fe5270+Fe5335)/2. The S/N ratio is given per Ångström. Internal uncertainties are given in the second line for each galaxy. The line indices have been aperture corrected to $2r_{\rm norm} = 1.19{\rm h}^{-1}$kpc, equivalent to $3\farcs4$ at the distance of the Coma cluster. The line indices are consistent with the Lick/IDS system and corrected to zero velocity dispersion.

TABLE A4

SPECTROSCOPIC PARAMETERS, MEAN VALUES

Galaxy	log σ	Hβ	Hβ_G	Mg$_1$	Mg$_2$	Mgb	<Fe>	References
1750	2.413	1.59	1.97	0.122	0.315	5.61	2.69	Dav87,L91,G92,LCS
	0.015	0.29	0.19	0.007	0.007	0.29	0.27	
1853	2.294	1.79	2.12	0.124	0.286	3.93	3.42	LCS
	0.021	0.21	0.15	0.005	0.007	0.23	0.20	
2000	2.286	···	1.84[a]	···	0.309	···	···	Dav87,L91,G92,C93
	0.017	···	0.20	···	0.013	···	···	
2091	2.102	···	···	···	0.272	···	···	L91,G92
	0.033	···	···	···	0.013	···	···	
2157	2.277	1.88	2.03	0.116	0.276	4.30	3.05	LCS
	0.019	0.19	0.13	0.005	0.006	0.20	0.18	
2237	1.997	2.25	2.22	0.072	0.238	3.97	2.78	LCS
	0.026	0.24	0.16	0.006	0.007	0.26	0.23	
2252	2.171	···	···	···	0.269	···	···	L91,G92
	0.022	···	···	···	0.013	···	···	
2259	2.008	2.55	2.88	0.089	0.216	3.44	2.75	LCS,FMOS
	0.033	0.24	0.16	0.006	0.007	0.26	0.23	
2347	2.184	2.36	2.44	0.102	0.258	3.87	3.39	Dres87,FMOS
	0.036	0.36	0.24	0.009	0.011	0.38	0.34	
2390	2.344	1.50	1.66	0.155	0.331	4.91	2.77	Dav87,LCS,FMOS
	0.018	0.13	0.09	0.003	0.004	0.13	0.12	
2393	2.124	1.82	2.03	0.048	0.169	3.17	2.08	LCS
	0.035	0.28	0.19	0.007	0.008	0.30	0.27	
2413	2.235	1.82	2.04	0.113	0.276	4.30	3.15	LCS
	0.023	0.23	0.15	0.006	0.007	0.24	0.21	
2417	2.325	2.36	2.19	0.101	0.282	4.48	2.90	Dres87,FMOS
	0.036	0.21	0.14	0.005	0.006	0.22	0.20	
2440	2.328	1.67	1.78	0.120	0.299	4.81	2.75	Dav87,FMOS
	0.025	0.15	0.10	0.004	0.004	0.15	0.14	
2489	1.965	···	···	···	0.256	···	···	Dres87
	0.036	···	···	···	0.013	···	···	
2495	2.106	2.13	2.31	0.101	0.261	4.19	2.68	LCS
	0.025	0.23	0.16	0.006	0.007	0.25	0.22	
2510	2.132	···	1.95[a]	···	0.256	···	···	Dres87,C93
	0.036	···	0.24	···	0.013	···	···	
2516	2.228	···	···	···	0.283	···	···	Dres87
	0.036	···	···	···	0.013	···	···	
2535	2.142	1.72	1.62	0.103	0.278	4.15	3.20	Dres87,FMOS
	0.036	0.47	0.32	0.011	0.014	0.49	0.43	
2541	2.227	1.87	1.92	0.115	0.285	4.74	2.89	Dav87,FMOS
	0.025	0.11	0.07	0.003	0.003	0.11	0.10	
2551	2.039	2.24	2.25	0.083	0.236	3.33	2.84	Dres87,FMOS
	0.036	0.24	0.16	0.006	0.007	0.25	0.22	
2584	1.975	···	2.23[a]	···	0.231	···	···	Dres87,C93
	0.036	···	0.32	···	0.013	···	···	
2629	2.188	2.30	2.35	0.118	0.284	4.53	2.75	LCS
	0.026	0.23	0.16	0.006	0.007	0.25	0.22	
2651	1.993	1.85	2.18	0.084	0.223	3.58	3.23	LCS
	0.028	0.24	0.16	0.006	0.007	0.26	0.23	
2654	2.204	···	1.93[a]	···	0.289	···	···	Dres87,C93
	0.036	···	0.24	···	0.013	···	···	
2670	1.997	···	···	···	0.264	···	···	L91,G92
	0.022	···	···	···	0.013	···	···	
2727	2.164	2.48	2.41	0.095	0.270	4.34	3.10	Dres87,FMOS
	0.036	0.27	0.19	0.007	0.008	0.29	0.26	
2776	2.112	2.07	2.24	0.110	0.268	4.10	3.09	LCS,FMOS
	0.024	0.11	0.08	0.003	0.003	0.12	0.11	
2794	2.151	···	···	···	0.264	···	···	Dav87
	0.025	···	···	···	0.013	···	···	
2795	2.346	···	1.98[a]	···	0.301	···	···	Dres87,C93
	0.036	···	0.22	···	0.013	···	···	
2798	2.308	1.67	2.06	0.114	0.283	4.27	2.83	Dav87,FMOS
	0.025	0.19	0.13	0.005	0.006	0.19	0.18	
2815	1.975	···	1.93[a]	···	0.235	···	···	Dres87,C93
	0.036	···	0.27	···	0.013	···	···	
2839	2.204	···	2.15[a]	···	0.304	···	···	Dav87,C93
	0.025	···	0.21	···	0.013	···	···	
2861	2.156	···	2.01[a]	···	0.296	···	···	Dres87,C93
	0.036	···	0.21	···	0.013	···	···	
2912	2.187	2.20	2.35	0.090	0.258	4.12	2.97	Dav87,LCS
	0.017	0.24	0.16	0.006	0.006	0.25	0.22	
2921	2.608	1.86	1.85	0.163	0.342	5.54	3.25	Dav87,L91,G92,LCS,FMOS
	0.014	0.07	0.05	0.002	0.002	0.07	0.06	
2922	2.257	1.73	2.09	0.133	0.303	5.16	3.42	Dav87,FMOS
	0.025	0.26	0.18	0.006	0.008	0.27	0.25	
2940	2.027	···	2.05[a]	···	0.285	···	···	Dav87,C93
	0.025	···	0.22	···	0.013	···	···	
2945	2.079	···	1.57[a]	···	0.261	···	···	Dres87,C93
	0.036	···	0.27	···	0.013	···	···	
2956	2.117	1.82	2.15	0.112	0.262	4.29	3.46	LCS
	0.027	0.29	0.19	0.007	0.009	0.30	0.27	
2975	2.178	2.09	2.12	0.107	0.265	4.16	2.68	Dav87,L91,G92,FMOS
	0.017	0.08	0.06	0.002	0.002	0.09	0.08	

TABLE A4—*Continued*

Galaxy	log σ	Hβ	Hβ_G	Mg_1	Mg_2	Mgb	<Fe>	References
3055	2.314	1.78	2.01	0.133	0.312	4.69	2.97	Dav87,L91,G92,FMOS
	0.017	0.16	0.11	0.004	0.005	0.17	0.15	
3068	1.979	1.71	2.11	0.077	0.224	3.71	2.45	LCS
	0.030	0.27	0.18	0.007	0.008	0.29	0.26	
3073	2.252	2.03	2.12	0.121	0.303	4.61	3.36	Dres87,FMOS
	0.036	0.14	0.10	0.004	0.004	0.15	0.14	
3084	2.081	···	1.67[a]	···	0.269	···	···	Dav87,C93
	0.025	···	0.23	···	0.013	···	···	
3165	2.225	2.28	2.32	0.095	0.251	3.94	2.82	Dres87,FMOS
	0.036	0.12	0.08	0.003	0.003	0.12	0.11	
3170	2.210	2.12	2.22	0.113	0.280	4.44	3.06	Dres87,FMOS
	0.036	0.15	0.10	0.004	0.004	0.15	0.14	
3178	2.118	···	···	···	0.278	···	···	Dres87
	0.036	···	···	···	0.013	···	···	
3201	2.261	2.15	2.18	0.098	0.260	3.92	2.97	Dav87,L91,G92,FMOS
	0.025	0.12	0.08	0.003	0.004	0.13	0.11	
3213	2.132	···	···	···	0.285	···	···	Dav87
	0.025	···	···	···	0.013	···	···	
3222	2.231	···	···	···	0.273	···	···	Dav87,L91,G92
	0.025	···	···	···	0.013	···	···	
3269	2.037	···	···	···	0.259	···	···	Dres87
	0.036	···	···	···	0.013	···	···	
3296	2.278	1.61	1.77	0.131	0.290	4.60	3.31	Dres87,FMOS
	0.036	0.23	0.16	0.006	0.007	0.24	0.22	
3328	2.147	2.08	2.33	0.047	0.223	4.22	2.91	LCS
	0.025	0.21	0.14	0.005	0.006	0.22	0.20	
3329	2.415	1.78	1.95	0.136	0.310	5.21	3.14	Dav87,L91,G92,LCS,FMOS
	0.016	0.12	0.08	0.003	0.004	0.13	0.12	
3352	2.328	···	1.90[a]	···	0.305	···	···	Dav87,C93
	0.025	···	0.20	···	0.013	···	···	
3367	2.193	1.85	2.00	0.120	0.287	4.79	2.50	Dres87,FMOS
	0.036	0.24	0.16	0.006	0.007	0.24	0.22	
3390	2.225	2.75	2.61	0.104	0.273	4.02	3.05	Dres87,FMOS
	0.036	0.33	0.22	0.008	0.010	0.35	0.31	
3400	2.337	2.14	2.27	0.156	0.318	4.66	3.19	Dres87,FMOS
	0.036	0.27	0.19	0.007	0.008	0.29	0.26	
3403	1.901	···	···	···	0.234	···	···	Dav87
	0.025	···	···	···	0.013	···	···	
3414	2.243	1.85	2.00	0.128	0.292	4.70	2.88	Dres87,FMOS
	0.036	0.22	0.15	0.005	0.006	0.22	0.20	
3423	2.418	···	1.49[a]	···	0.327	···	···	Dres87,C93
	0.036	···	0.18	···	0.013	···	···	
3433	2.016	···	2.23[a]	···	0.265	···	···	Dres87,C93
	0.036	···	0.29	···	0.013	···	···	
3471	2.001	···	2.34[a]	···	0.235	···	···	L91,G92,C93
	0.022	···	0.25	···	0.013	···	···	
3484	2.118	···	···	···	0.260	···	···	Dres87
	0.036	···	···	···	0.013	···	···	
3487	2.122	···	···	···	0.272	···	···	Dres87
	0.036	···	···	···	0.013	···	···	
3493	2.187	···	···	···	0.286	···	···	Dres87
	0.036	···	···	···	0.013	···	···	
3510	2.313	···	···	···	0.321	···	···	Dav87
	0.025	···	···	···	0.013	···	···	
3522	2.219	···	···	···	0.250	···	···	Dres87
	0.036	···	···	···	0.013	···	···	
3557	1.838	···	···	···	0.238	···	···	Dav87
	0.025	···	···	···	0.013	···	···	
3561	2.388	···	2.03[a]	···	0.294	···	···	Dres87,C93
	0.036	···	0.21	···	0.013	···	···	
3639	2.350	1.77	1.79	0.145	0.294	4.87	2.89	Dav87,FMOS
	0.025	0.37	0.25	0.009	0.011	0.38	0.35	
3656	2.116	1.54	1.96	0.077	0.231	3.76	2.60	LCS,FMOS
	0.031	0.21	0.14	0.005	0.006	0.22	0.20	
3660	2.129	2.13	1.98	0.107	0.268	4.11	2.64	Dres87,FMOS
	0.036	0.15	0.10	0.004	0.004	0.16	0.14	
3661	2.255	2.03	2.28	0.108	0.258	3.92	2.39	LCS
	0.025	0.24	0.16	0.006	0.007	0.26	0.23	
3664	2.297	···	1.93[a]	···	0.290	···	···	Dav87,C93
	0.025	···	0.20	···	0.013	···	···	
3730	2.297	1.57	1.94	0.143	0.306	4.50	3.11	Dav87,L91,G92,LCS
	0.015	0.27	0.18	0.007	0.007	0.28	0.25	
3733	2.261	···	···	···	0.345	···	···	Dres87
	0.036	···	···	···	0.013	···	···	
3739	2.180	···	···	···	0.296	···	···	Dav87
	0.025	···	···	···	0.013	···	···	
3761	2.276	2.10	2.20	0.102	0.268	4.40	3.13	Dres87,FMOS
	0.036	0.12	0.08	0.003	0.003	0.12	0.11	
3782	2.082	···	2.10[a]	···	0.281	···	···	Dres87,C93
	0.036	···	0.23	···	0.013	···	···	
3792	2.390	1.82	1.99	0.147	0.334	5.36	2.71	Dav87,L91,G92,FMOS
	0.017	0.23	0.16	0.006	0.007	0.24	0.22	

TABLE A4—*Continued*

Galaxy	log σ	Hβ	Hβ_G	Mg$_1$	Mg$_2$	Mgb	<Fe>	References
3818	2.298	1.63	1.91	0.109	0.259	4.21	2.70	LCS
	0.025	0.26	0.18	0.006	0.008	0.28	0.25	
3851	1.901	...	...	...	...	...	...	L91
	0.033	...	...	...	...	...	...	
3879	2.136	2.10	2.29	0.117	0.260	4.11	2.96	LCS
	0.026	0.25	0.17	0.006	0.008	0.27	0.24	
3914	2.184	...	...	...	0.280	...	...	Dav87,L91,G92
	0.017	...	...	...	0.013	...	...	
3958	2.142	...	2.20[a]	...	0.282	...	...	L91,G92,C93
	0.022	...	0.24	...	0.013	...	...	
3972	2.170	...	2.27[a]	...	0.257	...	...	Dres87,C93
	0.036	...	0.24	...	0.013	...	...	
3997	2.327	1.57	1.83	0.124	0.271	4.18	2.49	LCS
	0.027	0.25	0.17	0.006	0.008	0.26	0.24	
4017	2.263	2.24	1.94	0.116	0.302	3.79	2.37	Dav87,L91,FMOS
	0.021	0.77	0.53	0.019	0.023	0.83	0.75	
4130	2.262	1.97	2.29	0.124	0.276	4.71	3.02	LCS
	0.023	0.23	0.16	0.006	0.007	0.24	0.22	
4156	2.115	2.30	2.33	0.056	0.164	2.57	2.01	LCS,FMOS
	0.035	0.08	0.06	0.002	0.002	0.09	0.08	
4206	2.068	1.91	2.22	0.084	0.231	4.26	2.62	LCS
	0.024	0.23	0.16	0.006	0.007	0.24	0.22	
4230	2.242	2.10	2.15	0.133	0.278	4.34	2.83	L91,G92,FMOS
	0.022	0.25	0.17	0.006	0.008	0.26	0.24	
4308	1.973	1.92	2.10	0.048	0.199	3.69	2.73	LCS
	0.034	0.30	0.21	0.007	0.009	0.32	0.29	
4313	2.128	1.80	2.17	0.095	0.249	4.29	2.80	LCS
	0.026	0.25	0.17	0.006	0.007	0.26	0.23	
4315	2.227	1.35	1.59	0.130	0.287	4.37	2.77	L91,G92,FMOS
	0.022	0.13	0.09	0.003	0.004	0.14	0.12	
4379	2.267	1.74	2.13	0.114	0.283	4.24	2.74	LCS
	0.016	0.14	0.10	0.004	0.004	0.15	0.13	
4391	1.968	2.25	2.41	0.075	0.211	3.50	2.57	LCS,FMOS
	0.027	0.17	0.12	0.004	0.005	0.19	0.17	
4499	2.217	1.82	1.86	0.096	0.254	4.49	2.94	LCS
	0.026	0.25	0.17	0.006	0.007	0.26	0.23	
4588	2.013	...	...	...	0.240	...	...	L91,G92
	0.022	...	...	...	0.013	...	...	
4626	2.090	1.38	1.59	0.089	0.249	4.83	2.77	LCS
	0.044	0.45	0.31	0.011	0.014	0.46	0.42	
4648	2.225	...	...	...	0.274	...	...	L91,G92
	0.033	...	...	...	0.013	...	...	
4653	2.195	1.93	2.31	0.120	0.295	4.83	2.83	LCS
	0.021	0.21	0.14	0.005	0.007	0.22	0.20	
4664	2.140	2.27	2.29	0.091	0.251	3.91	2.99	LCS
	0.025	0.24	0.16	0.006	0.007	0.25	0.22	
4679	1.852	2.64	2.89	0.077	0.220	3.28	2.29	LCS
	0.032	0.27	0.18	0.007	0.008	0.29	0.26	
4792	2.175	1.98	2.22	0.092	0.255	4.72	2.62	LCS
	0.034	0.29	0.20	0.007	0.009	0.31	0.28	
4794	2.272	1.60	1.78	0.116	0.298	4.77	2.74	LCS
	0.029	0.26	0.18	0.006	0.008	0.27	0.24	
4806	2.304	1.84	2.03	0.127	0.286	4.42	3.14	Dav87,LCS,FMOS
	0.019	0.17	0.12	0.004	0.005	0.18	0.16	
4822	2.412	1.65	1.80	0.144	0.317	4.98	2.79	Dav87,LCS,FMOS
	0.017	0.14	0.09	0.003	0.004	0.14	0.13	
4829	2.370	...	1.73[a]	...	0.323	...	...	L91,G92,C93
	0.033	...	0.19	...	0.013	...	...	
4866	2.081	2.03	2.15	0.101	0.260	4.19	2.92	LCS,FMOS
	0.029	0.21	0.14	0.005	0.006	0.22	0.20	
4907	2.262	1.43	1.76	0.105	0.269	4.44	2.21	LCS
	0.030	0.25	0.17	0.006	0.007	0.25	0.23	
4918	1.878	-6.28	-5.38	0.037	0.117	3.12	1.50	LCS
	0.048	0.35	0.24	0.007	0.008	0.31	0.28	
4928	2.406	1.36	1.85	0.139	0.312	4.74	2.60	Dav87,L91,G92,LCS
	0.017	0.24	0.16	0.006	0.006	0.25	0.22	
5051	2.347	...	2.18[a]	...	0.305	...	...	L91,G92,C93
	0.033	...	0.25	...	0.013	...	...	

NOTE.— Galaxy identifications from Godwin et al. (1983). References: Dav87 – Davies et al. (1987); Dres87 – Dressler (1987); L91 – Lucey et al. (1991); G92 – Guzmán et al. (1992); C93 – Caldwell et al. (1993); LCS – derived from the LCS spectra; FMOS – derived from the FMOS spectra. The mean values include all measurements from the noted references; see JFK95b for the description of how the literature data were calibrated to a consistent system. [a] Hβ_G is derived from Hδ from Caldwell et al. (1993). <Fe>=(Fe5270+Fe5335)/2. Internal uncertainties are given in the second line for each galaxy. The velocity dispersions and the line indices have been aperture corrected to $2r_{\rm norm} = 1.19{\rm h}^{-1}$kpc, equivalent to $3\farcs4$ at the distance of the Coma cluster. The line indices are consistent with the Lick/IDS system and corrected to zero velocity dispersion.